



Government of **Western Australia**  
Department of **Mines, Industry Regulation and Safety**

RECORD 2017/9

# METAMORPHOSED VMS MINERALIZATION AT WHEATLEY, SOUTHWEST WESTERN AUSTRALIA

by  
LY Hassan



Geological Survey of  
Western Australia



Government of **Western Australia**  
Department of **Mines, Industry Regulation and Safety**

**Record 2017/9**

# **METAMORPHOSED VMS MINERALIZATION AT WHEATLEY, SOUTHWEST WESTERN AUSTRALIA**

by  
**LY Hassan**

**Perth 2017**



**Geological Survey of  
Western Australia**

**MINISTER FOR MINES AND PETROLEUM**  
**Hon Bill Johnston MLA**

**ACTING DIRECTOR GENERAL, DEPARTMENT OF MINES, INDUSTRY REGULATION AND SAFETY**  
**David Smith**

**EXECUTIVE DIRECTOR, GEOLOGICAL SURVEY OF WESTERN AUSTRALIA**  
**Rick Rogerson**

#### **REFERENCE**

**The recommended reference for this publication is:**

Hassan, LY 2017, Metamorphosed VMS mineralization at Wheatley, southwest Western Australia: Geological Survey of Western Australia, Record 2017/9, 39p.

**National Library of Australia Card Number and ISBN 978-1-74168-766-8**

Grid references in this publication refer to the Geocentric Datum of Australia 1994 (GDA94). Locations mentioned in the text are referenced using Map Grid Australia (MGA) coordinates, Zone 50. All locations are quoted to at least the nearest 100 m.

#### **Disclaimer**

This product was produced using information from various sources. The Department of Mines, Industry Regulation and Safety (DMIRS) and the State cannot guarantee the accuracy, currency or completeness of the information. DMIRS and the State accept no responsibility and disclaim all liability for any loss, damage or costs incurred as a result of any use of or reliance whether wholly or in part upon the information provided in this publication or incorporated into it by reference.

#### **Published 2017 by Geological Survey of Western Australia**

This Record is published in digital format (PDF) and is available online at <[www.dmp.wa.gov.au/GSWApublications](http://www.dmp.wa.gov.au/GSWApublications)>.

#### **Further details of geological products and maps produced by the Geological Survey of Western Australia are available from:**

Information Centre  
Department of Mines, Industry Regulation and Safety  
100 Plain Street  
EAST PERTH WESTERN AUSTRALIA 6004  
Telephone: +61 8 9222 3459 Facsimile: +61 8 9222 3444  
[www.dmp.wa.gov.au/GSWApublications](http://www.dmp.wa.gov.au/GSWApublications)

**Cover image:** Elongate salt lake on the Yilgarn Craton — part of the Moore–Monger paleovalley — here viewed from the top of Wownaminy Hill, 20 km southeast of Yalgoo, Murchison Goldfields. Photograph taken by I Zibra for the Geological Survey of Western Australia

## Contents

Abstract .....	1
Introduction .....	1
Geological setting.....	4
Methods.....	5
HyLogger .....	5
Petrography .....	6
Electron microprobe (WDS) analyses.....	6
SEM analyses .....	6
Geochemistry .....	6
Mineralization and lithologies intersected .....	6
Kingsley Prospect.....	6
WPD04 .....	6
WPD07 .....	7
WPD02.....	13
WPD13.....	16
Jack Prospect.....	16
WPD03.....	16
Chemistry of the host succession .....	18
Mineral distribution and chemistry .....	23
Garnet.....	23
Gahnite .....	26
Staurolite .....	26
Kyanite .....	26
Sillimanite .....	30
Andalusite .....	30
Amphiboles .....	30
Discussion .....	31
Protoliths of the host succession .....	31
Amphibolite .....	31
Compositionally layered rocks.....	31
?Felsic volcanic and volcanic breccia .....	31
Felsic gneiss.....	31
Tectonic setting .....	31
Morphology of the mineralization .....	32
Evidence of alteration .....	33
Evidence for pre-metamorphic origin of the mineralization.....	34
Age of mineralization.....	35
Uses and limitations of the HyLogger data.....	35
Exploration vectors .....	35
Conclusions.....	37
Acknowledgements .....	37
References .....	37

## Appendices

1. Allowed minerals — SWIR
2. Allowed minerals — TIR
3. Lithological logs
4. Garnet electron microprobe analyses and composition
5. Garnet SEM analyses and composition
6. Staurolite analyses

Appendices are available on the accompanying zip file.



## Figures

1.	Regional interpreted geological map showing geochronology sites and location of the Wheatley project area .....	2
2.	Orthophoto of the Wheatley project area showing prospects, mineral occurrences and drillholes .....	3
3.	Photomicrographs of main zone of mineralization in WPD04 .....	8
4.	Photomicrograph of galena replacing biotite along cleavage .....	9
5.	Photomicrographs of second zone of mineralization in WPD04 .....	9
6.	HyLogger, lithology and assay data for WPD04 .....	10
7.	Core and thin section of compositionally layered rock .....	11
8.	Photomicrographs of amphibolite and mafic gneiss .....	11
9.	Core of pegmatite with coarse-grained tourmaline .....	11
10.	Photomicrographs of minerals in gneiss beneath mineralization .....	12
11.	Thin section of metagabbro .....	13
12.	Reflected light image of massive sulfide mineralization in WPD07 .....	13
13.	Reflected light image of disseminated arsenopyrite, pyrite and pyrrhotite adjacent to quartz vein in possible shear zone .....	13
14.	HyLogger, lithology and assay data for WPD07 .....	14
15.	Photomicrographs of alteration zone beneath mineralization in WPD07 .....	15
16.	Core and photomicrographs of possible felsic volcanic rock and volcanic breccia at bottom of WPD07 .....	15
17.	Reflected light images of mineralization from WPD02 .....	16
18.	HyLogger, lithology and assay data for WPD02 .....	17
19.	Core and photomicrograph of tourmaline-rich horizon below mineralization in WPD02 .....	18
20.	Thin section of felsic rock containing andalusite and minor tourmaline in WPD02 .....	18
21.	Thin section of gabbro with randomly orientated plagioclase crystals in WPD02 .....	18
22.	HyLogger, lithology and assay data for WPD13 .....	19
23.	Reflected light images of mineralization infilling fractures in gabbro WPD03 at the Jack Prospect .....	20
24.	HyLogger, lithology and assay data for WPD03 .....	21
25.	Core and thin section of layered mafic intrusion in WPD03 .....	22
26.	Amphibolites and mafic intrusions plotted on volcanic discrimination diagram of Pearce (1996) .....	22
27.	Interpreted felsic volcanic rocks and gneiss plotted on the volcanic classification diagram of Winchester and Floyd (1977) .....	23
28.	Mantle-normalized immobile element abundances for various rock types from Wheatley .....	24
29.	HyLogger interpretations of variation in garnet composition downhole vs simplified log for WPD04 .....	25
30.	Downhole match for staurolite in WPD04 with SWIR spectra of staurolite from the United States Geological Survey (USGS) spectral library and with the TIR spectra from the John Hopkins University (JHU) spectral library versus simplified log .....	29
31.	Amphibolites plotted on Th/Yb vs Nb/Yb discrimination plot of Pearce (2008) .....	32
32.	Amphibolites plotted on Th–Zr–Nb discrimination plot of Wood (1980) .....	33
33.	Weighted downhole distribution of tourmaline in WPD02 according to SWIR and TIR versus simplified log .....	36
34.	Spectra over zone of massive tourmaline in WPD02 compared with the SWIR spectra for Fe-tourmaline in TSG .....	36

## Tables

1.	Geochronology .....	4
2.	Wheatley Prospect drill collars .....	5
3.	Wheatley geochemistry (on accompanying zip file) .....	
4.	Garnet composition .....	27
5.	Staurolite composition .....	29
6.	Sillimanite microprobe analyses .....	30
7.	Amphibole composition .....	30

# Metamorphosed VMS mineralization at Wheatley, southwest Western Australia

by

LY Hassan

## Abstract

At the Kingsley Prospect near Wheatley, southwest Western Australia, zinc-rich base metal mineralization occurs at the contact between felsic gneiss and a more mafic succession of hornblende-rich compositionally layered rocks and amphibolite over a strike length of 1.6 km. The presence of gahnite indicates that the mineralization pre-dated the amphibolite grade metamorphism and, together with the stratigraphic control and association with volcanic rocks, supports a VMS origin for the mineralization.

Trace element geochemistry indicates that the amphibolites range from basalt to basaltic andesite in composition. On a plot of Th/Yb vs Nb/Yb, used to discriminate between various processes of crust/mantle interaction, some of the amphibolites have compositions close to enriched mid-oceanic ridge basalt (EMORB) while others plot almost vertically above a mantle array. The vertical trend could be indicative of variable amounts of crustal contamination (possibly related to subduction) or to Th mobility during high-grade metamorphism. A rifted back-arc basin setting is consistent with the trace element data and rock types observed but more work is required to verify the tectonic setting.

Sillimanite, kyanite, staurolite and garnet in the gneisses below the mineralization may reflect metamorphosed argillic alteration and the presence of tourmaline may be indicative of exhalative boron. HyLogger data suggest that garnet in gneisses below the mineralization is compositionally distinct from that in the amphibolites and hornblende-bearing compositionally layered rocks above the mineralization. Microprobe and SEM analysis confirm this (although the compositional differences are not as marked as indicated by the HyLogger) and show that garnet composition is generally related to host rock composition. However, garnet from a mineralized sample contained the highest content of spessartine.

Vectors to mineralization include gahnite, zinc-bearing staurolite and spessartine-rich garnet in stream samples; the presence of abundant kyanite since it likely reflects alteration related to mineralization; and anomalous Bi concentrations in laterite because of the observation of native Bi inclusions in galena. EM surveys have been useful in detecting sulfides at the Kingsley Prospect.

**KEYWORDS:** gahnite, garnet, hydrothermal alteration, massive sulphide deposits, metamorphism, spectroscopy, staurolite, volcanic hosted deposits, zinc

## Introduction

The Wheatley project is situated south-southeast of the townsite of Wheatley about 250 km south of Perth and 17 km west-northwest of Manjimup within the South West Terrane of the Yilgarn Craton (Fig. 1).

Earliest exploration in the area was for kyanite. Within the area, there are a number of shallow pits and shafts in weathered kyanite-quartz schist but all kyanite production was from eluvial boulders (Ellis, 1948). A total of 4228 tonnes of eluvial kyanite was mined from the area between 1946 and 1948. In 1993, Pancontinental Mining intersected gold mineralization (up to 2 m at 2.75 ppm Au) at the fractured contact between dark biotite-rich feldspar gneiss and lighter coloured feldspar-rich biotite gneiss when testing a gold-arsenic anomaly by reverse circulation drilling (Carlson and Harrison, 1993).

The zinc spinel gahnite, together with scheelite, was identified in a stream sample by BHP Minerals Pty Ltd (Hart et al., 2000) while following up Pb-As-W and Sb laterite lag anomalies. These anomalies were identified by CSIRO in the early 1980s and other anomalies were identified by Pancontinental Mining.

Massive sulfides interpreted to be metamorphosed volcanogenic massive sulfide (VMS) mineralization were intersected in diamond drillcore from the Kingsley Prospect between 2003 and 2007 as a follow up to earlier laterite lag sampling and aerial and ground EM surveys (Johnston, 2003; Griggs, 2004; Savage, 2007). Minor sulfides were also intersected in drillcore from the Jack Prospect. The locations of these prospects and drillholes are shown on Figure 2. Johnson (2003) reported wide zones containing abundant aluminosilicates, garnet, staurolite, and cordierite beneath the sulfide zones, and interpreted these zones to be the metamorphosed equivalents of footwall alteration beneath VMS deposits. Core from these diamond drillholes was donated to the Geological Survey of Western Australia (GSWA) Perth Core Library by Teckcominco Australia Pty Ltd and Hampton Hill Mining NL. That core formed the basis of this study which was aimed at verifying that the mineralization was indeed metamorphosed VMS mineralization, and the nature of the alteration and host rocks using hyperspectral HyLogger data supported by conventional logging and petrography. The study was part of a broader study of VMS deposits in the western part of the Yilgarn by the Mineral Systems team at GSWA, and was aimed at building genetic models for the environment of ore formation and providing useful vectors for exploring in greenfields areas.

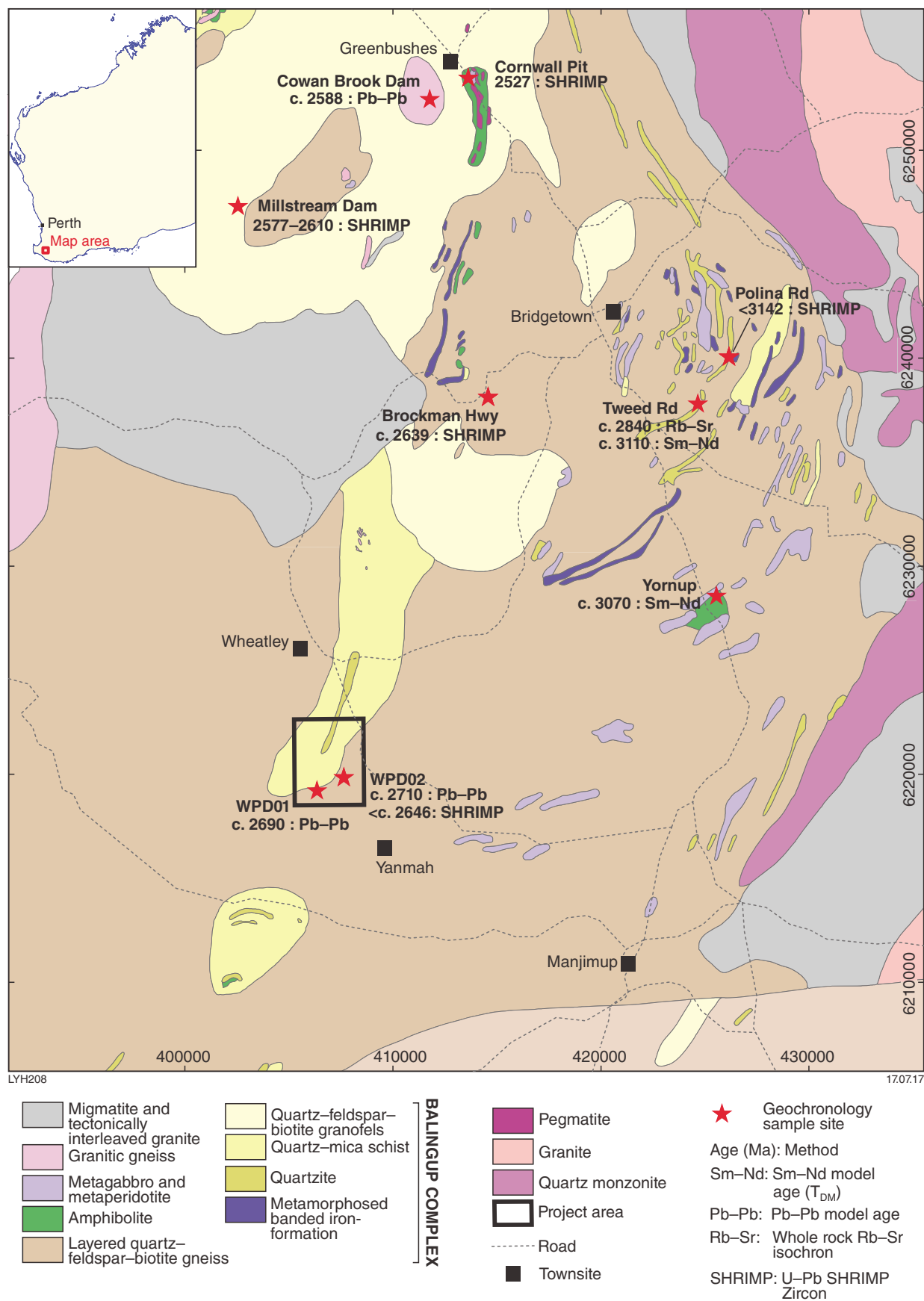


**Figure 1. Regional interpreted geological map of a portion of the Balingup complex (based on Hassan et al., 1998) showing geochronology sites and the location of the Wheatley project area**



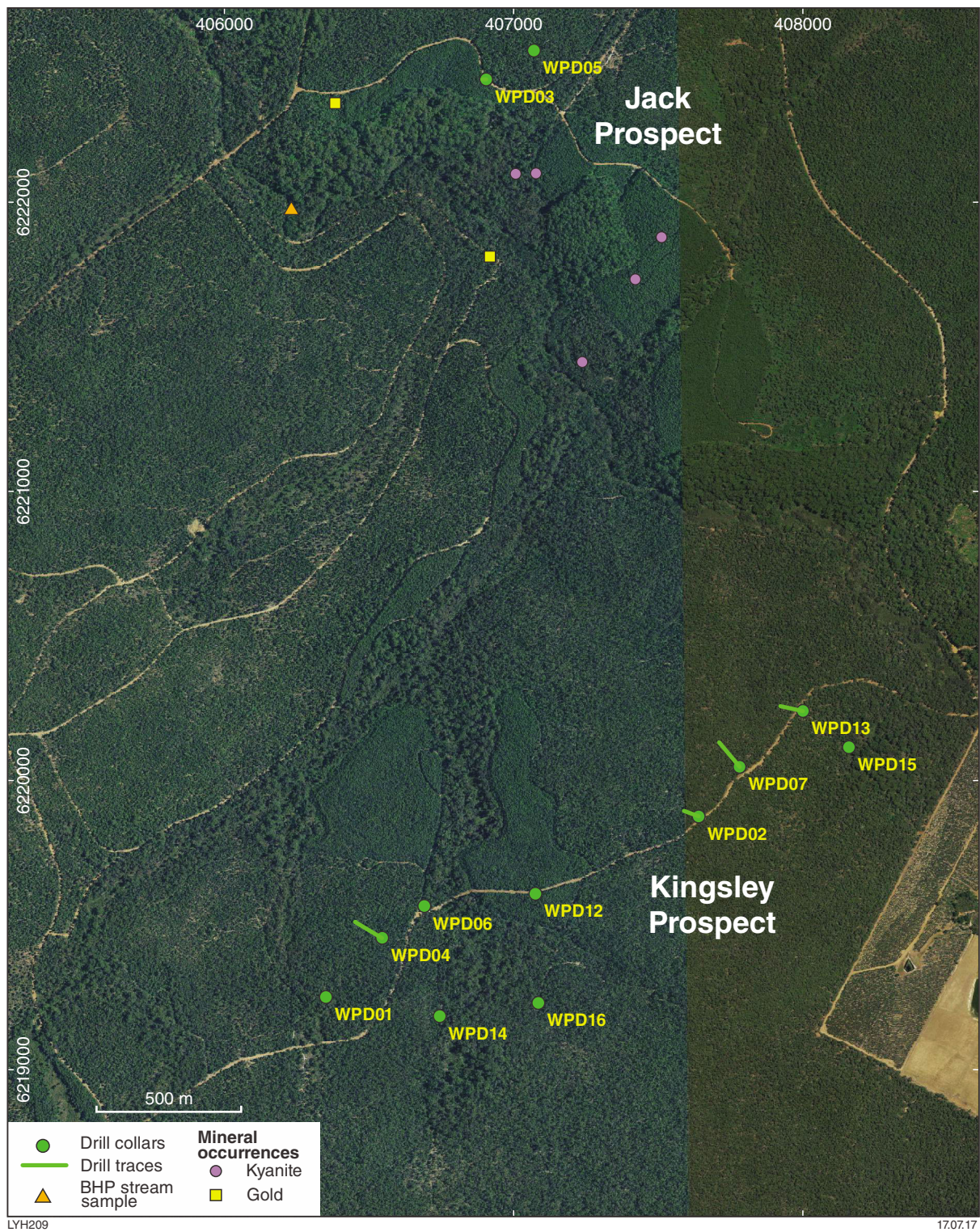


Figure 2. Orthophoto of the Wheatley project area showing prospects, mineral occurrences and drillholes



## Geological setting

The Wheatley Prospects fall within an area of high-grade metamorphic rocks in the southwestern part of the Yilgarn Craton informally referred to as the Balingup complex by Hassan (1998) and previously referred to as either the Balingup Metamorphic Belt (Wilde, 1980; Gee et al., 1981) or as the Balingup Gneiss Complex (Myers, 1990). The Balingup complex forms part of the South West Terrane of Tyler and Hocking (2001) and Cassidy et al. (2006). Wilde (1980) described the complex as consisting mainly of metasedimentary rocks including interlayered quartzite, quartz-mica schist, quartz-feldspar-biotite (–garnet) gneiss, and banded iron-formation, together with minor layers of quartzofeldspathic gneiss, amphibolite, calc-silicate gneiss, and ultramafic rock. These rocks have been isoclinally folded and metamorphosed predominantly to amphibolite facies but locally to granulite facies. An interpretation of the basement geology of a portion of the Balingup complex (Hassan et al., 1998) is given in Figure 1. It should be noted that this map was originally compiled from a combination of published 1:250 000 geological map sheets (Lowry et al., 1983; Wilde and Walker, 1984), maps in open-file statutory exploration reports, and the aeromagnetic data available at the time, and is in need of revision in the light of results from this study.

The age of the Balingup complex is uncertain. The locations of samples that have been dated are shown on Figure 1 and tabulated in Table 1. Layered gneiss from Tweed Road (5.8 km southeast of Bridgetown) and gneiss from Yornup (14.4 km south-southeast of Bridgetown) gave whole-rock Sm–Nd model ages ( $T_{DM}$ ) of 3.11 and 3.07 Ga respectively (Fletcher et al., 1983). The Tweed Road sample had previously been dated by DA Nieuland in 1977 using the Rb–Sr whole-rock isochron method (Fletcher et al., 1984) at  $2.84 \pm 0.2$  Ga. Fletcher et al. (1984) interpreted the Rb–Sr whole-rock isochron age as dating the amphibolite facies metamorphism whereas the Sm–Nd data indicated a mean mantle extraction age of 3.1 Ga. Zircons from a quartzite at Polina Road, 6 km east-southeast of Bridgetown gave U–Pb SHRIMP zircon ages ranging from c. 3142 to 3365 Ma indicating a maximum depositional age of 3142 Ma (or a more conservative estimate of 3202 Ma if one zircon is excluded; Lu et al., 2016). A sample composed dominantly of recrystallized quartz, microcline, plagioclase and micas taken from the depth interval 235.22 – 237.05 m in diamond drillhole WPD02 from the study area at Wheatley gave U–Pb SHRIMP zircon ages which ranged from about 2700 to 2600 Ma with a prominent age peak around 2646 Ma (Sircombe et al., 2007). The sample was interpreted by Sircombe et al. (2007) to be a psammite with a maximum age of deposition of c. 2646 Ma. In the current study, the sample interval was logged as felsic volcanic rock, but regardless of the protolith origin, the protolith is significantly younger than the ages reported for metasedimentary rocks from the Balingup complex by Fletcher et al. (1984) and Lu et al. (2016). Disseminated low-grade sulfide mineralization from diamond drillholes WPD01 and WPD02 from Wheatley gave model Pb/Pb ages of c. 2690 Ma and c. 2710 Ma, respectively (Denton et al., 2003). A sample of quartz-feldspar-mica gneiss from Brockman Highway, 7 km southwest of Brookton,

Table 1. Regional geochronology for a portion of the Balingup complex

ID	Sample no.	Easting	Northing	Zone	Location	Source	Description	Age (Ma)	Method
1	76-181	424579	6237839	50	Tweed Rd	Fletcher et al. (1983)	Layered gneiss	3110	Sm–Nd model age ( $T_{DM}$ )
2	76-181	424579	6237839	50	Tweed Rd	Fletcher et al. (1983)	Layered gneiss	2840 $\pm$ 200	Whole rock Rb–Sr isochron
3	54161A	425549	6228605	50	Yornup	Fletcher et al. (1983)	Gneiss	3070	Sm–Nd model age ( $T_{DM}$ )
4	184116	426155	6240097	50	Polina Rd	Lu et al. (2016)	Quartzite	< c. 3142	U–Pb SHRIMP zircon age
5	2004968001A	407640	6219876	50	Wheatley WPD02	Sircombe et al. (2007)	Metapsammite	< c. 2646	U–Pb SHRIMP zircon age
6	WP039	406350	6219250	50	Wheatley WPD01	Denton et al. (2003)	Mineralization	c. 2690	Pb–Pb model age ( $T_{DM}$ )
7	WP094	407640	6219876	50	Wheatley WPD02	Denton et al. (2003)	Mineralization	c. 2710	Pb–Pb model age
8	184117	414574	6238156	50	Brockman Hwy	Lu et al. (2015)	Granite gneiss	2639 $\pm$ 6	U–Pb SHRIMP zircon age
9		411773	6252480	50	Cowan Brook Dam	Partington et al. (1995)	Granite	c. 2588	Pb–Pb model age ( $T_{DM}$ )
10		402547	6247336	50	Millstream Dam	Partington et al. (1995)	Granite	2577–2610	U–Pb SHRIMP zircon age
11		413073	6253507	50	Cornwall Pit	Partington et al. (1995)	Pegmatite	2527 $\pm$ 2	U–Pb SHRIMP zircon age

gave U–Pb SHRIMP zircon ages ranging from c. 2628 to 2751 Ma (Lu et al., 2015). The sample analysed by Lu et al. (2015) was interpreted as granite gneiss with a magmatic crystallization age of  $2639 \pm 2$  Ma and with inherited zircons having ages of 2751–2701 Ma. An alternative interpretation would be that the gneiss is metasedimentary in origin (Wilde, 1980; Gee et al., 1981) and that the c. 2639 Ma date represents the maximum age of deposition.

Granitic rocks intruding the gneisses include the Cowan Brook Dam granitic rock which gave a whole-rock Pb–Pb age of  $2588 \pm 93$  Ma and the Millstream Dam granitic rock which gave a U–Pb SHRIMP zircon age of  $2577 \pm 4$  Ma (Partington et al., 1995). The Greenbushes pegmatite is significantly younger than the granitic rocks with a U–Pb SHRIMP zircon age of  $2527 \pm 2$  Ma (Partington et al., 1995).

## Methods

Core from four diamond drillholes at the Kingsley Prospect (WPD02, WPD04, WPD07 and WPD013) and one from the Jack Prospect (WPD03) were used in the current study. The locations of these drillholes are shown on Figure 2 and tabulated in Table 2. The core was logged conventionally as well as hyperspectrally using the HyLogger.

## HyLogger

Core from the five selected drillholes was scanned with the HyLogger at GSWA's core library in Carlisle using short wave infrared (SWIR), visible near infrared (VNIR) and thermal infrared (TIR) spectrometers. The HyLogger data were analysed using The Spectral Geologist (TSG), a program developed by CSIRO Earth Science and Resource Engineering and marketed by AusSpec International Pty Ltd. This program compares the measured spectra with the spectra of known minerals

and provides a system-generated interpretation of the mineralogy for each interval analysed (approximately 8 mm) (Pontual, 2008; Hancock et al., 2013). The three main minerals contributing to the spectra are calculated for each interval for the TIR spectrum and the two main minerals are calculated for the SWIR spectrum. A summary plot is calculated by averaging these minerals (or mineral groups) over a larger chosen interval (1–3 m depending on the length of the drillhole). SWIR is best for identifying mica, chlorite and clay minerals whereas TIR is best at identifying quartz, feldspar, pyroxene, garnet and phosphate. Both can identify Ca-amphiboles, talc and carbonates (Hancock et al., 2013). Visible near infrared (VNIR) is good at identifying iron oxides and rare earth minerals (Morin-Ka, 2012; Hancock et al., 2013).

Given the overlap between absorption features from different minerals, particularly for TIR, it is not surprising that the system-generated interpretation of minerals commonly requires further interpretation. Fortunately, TSG has the provision to allow or reject minerals in cases where thin-section studies provide independent information about a mineral's presence. Appendix 1 and 2 give the list of allowed and not allowed minerals used for the Wheatley core for TIR and SWIR respectively, determined by trial and error and using petrology as a guide. These tables are not perfect because in some instances minerals are suggested by TSG to be present in areas of drillcore where they are known, from thin section, to be absent; however, these minerals are required to be activated in TSG because they are present in other parts of the core. For example, pyroxenes are present in some of the intrusions but not in the gneisses even though TSG in places shows them in the gneisses. Chlorite was occasionally observed as a retrograde product but the TIR summary plots commonly showed abundant chlorite where biotite was the only ferromagnesian mineral observed in thin section. As SWIR is more reliable at identifying chlorite than TIR, chlorite was left on in SWIR but turned off in TIR. For similar reasons, clay minerals were turned off in TIR but turned on in SWIR.

**Table 2. Wheatley Prospect drill collars**

Hole ID units	Prospect	Easting	Northing	Zone	RL (m)	Max depth (m)	Dip	Azimuth
WPD01	WHT-001	406350	6219250	50	235.97	212	-75	350
WPD02	WHT-002	407640	6219876	50	255.78	237.5	-75	290
WPD03	Jack	406905	6222426	50	249.27	180	-85	270
WPD04	WHT-001	406545	6219455	50	238.65	220.5	-60	300
WPD05	Jack	407070	6222526	50	242.83	199.5	-60	287
WPD06	WHT-001	406690	6219565	50	235.74	199.4	-60	348
WPD07	WHT-002	407781	6220047	50	254.29	220.5	-60	320
WPD12	WHT-001	407075	6219608	50	240.63	120.1	-60	360
WPD13	WHT-002	408000	6220240	50	241.33	156.3	-60	300
WPD14	WHT-001	406744	6219184	50	242.86	347.4	-60	329
WPD15	WHT-002	408160	6220115	50	228.72	257.6	-60	296
WPD16	WHT-001	407085	6219230	50	245.53	330.1	-60	5

The scatter plot tab in TSG allows for individual minerals to be plotted downhole using either the first or second (or third in the case of TIR) most abundant mineral detected in each 8 mm interval. This was used for looking at variation in garnet composition downhole. Where a particular mineral is not in the TSG library, spectral matching with another spectral library can be carried out and the results plotted downhole as above. This was used for looking at the staurolite abundance downhole.

Company assay data and simplified geological drillhole logs were also imported into TSG and displayed along with the other scatter plots.

## Petrography

A total of 34 thin sections, 129 polished thin sections and three polished blocks was examined using an Olympus BX51 microscope fitted with a digital camera in order to understand the nature of the mineralization and host rocks, and to check and place constraints on the HyLogger data.

## Electron microprobe (WDS) analyses

Selected minerals were analysed using the JEOL 8530F microprobe at the Centre for Microscopy, Characterisation and Analysis, The University of Western Australia. This microprobe is equipped with five wavelength-dispersive crystal spectrometers (WDS), one JEOL silicon-drift energy-dispersive spectrometer (EDS) and a reflected-light optical microscope for focusing. Prior to analysis, all sections were cleaned and carbon coated. The microprobe was operated at a voltage of 20 kV and current of 20 nA with a take-off angle of 40° and a fully focused beam. Counting times of 20 seconds on-peak for all elements were employed and mean atomic number (MAN) background corrections employed throughout (Donovan and Tingle, 1996). Calibration standards included wollastonite for Si and Ca, rutile for Ti, magnetite for Fe, corundum for Al, periclase for Mg, jadeite for Na, orthoclase for K, ZnO for Zn, Cr<sub>2</sub>O<sub>3</sub> for Cr and pure Mn metal for Mn. The element abundances were acquired using analysing crystals TAP for Si K $\alpha$ , Al K $\alpha$ , Mg K $\alpha$  and Na K $\alpha$ , PET for Ca K $\alpha$ , LiFH for Ti K $\alpha$  and Cr K $\alpha$  and LiF for Fe K $\alpha$ , Zn K $\alpha$ , and Mn K $\alpha$ . The atomic number effects (ZAF) matrix correction procedure was employed throughout.

## SEM analyses

As scanning electron microscope (SEM) energy dispersive X-ray spectroscopy (EDS) analysis is much faster than electron microprobe (WDS) analysis, many garnets and some other minerals were analysed using a FEI XL40 SEM fitted with a Bruker X-flash 5030 EDS at the Earth Science and Resource Engineering division of CSIRO at Kensington, Western Australia. Results were recalculated to 100% using the Quantax Esprit EDS program of Bruker Nano GmbH, Germany.

## Geochemistry

Major element geochemistry cannot be used for classification or determination of the tectonic environment where the rocks are likely to have been altered. However, many trace elements including rare earth elements (REE) and high field strength elements (HFSE) are typically immobile during alteration and metamorphism up to lower amphibolite facies (Pearce, 1996), although not necessarily up to the metamorphic grades found at Wheatley. Provided accurate analyses are made and there has been no fractionation of the trace elements during metamorphism, trace elements can be used to classify rocks (Winchester and Floyd, 1977; Pearce, 1996) and to discriminate between rocks formed in different geological settings (Pearce and Cann, 1971, 1973; Wood et al., 1979; Wood, 1980; Sun and McDonough, 1989; Rollinson, 1993; Pearce, 1996, 2008; Swinden, 1996; Kerrich and Wyman, 1997).

Selected samples were submitted to GSWA's Carlisle laboratory where they were crushed and milled using a tungsten carbon mill. Morris (2007) showed that there was negligible contamination of Bunbury Basalt samples milled in this way for the REE and HFSE of interest. Powdered aliquots were then submitted to BV Minerals (Ultratrace) at Canning Vale, Western Australia for analysis of whole-rock geochemistry by X-ray fluorescence (XRF), and trace elements by laser ablation inductively coupled plasma mass spectroscopy (LA-ICP-MS) of a fragment of the XRF Li<sub>2</sub>B<sub>4</sub>O<sub>7</sub> fusion disk. The fusion process increases the homogeneity of the sample in the form of a glass, whereas ablating the glass disk to generate trace element data avoids issues with acid digestion of the sample prior to presentation to the ICP (Günther et al., 2001).

This method also addresses problems associated with incomplete dissolution of refractory elements (Watkins and Nolan, 1990; Jenner, 1996; Kerrich and Wyman, 1997; Kerrich and Said, 2011). Duplicates and standards submitted with the samples (Table 3) showed that there was reasonable accuracy and precision for the elements of interest with the blank containing less than three times the lower detection limit.

Base metal analyses used in the logs were those reported by the companies (Johnston, 2003; Griggs, 2004; Savage, 2007). The method is not reported but it is likely to have been a three-acid digest followed by atomic absorption spectroscopy (AAS) or ICP.

## Mineralization and lithologies intersected

### Kingsley Prospect

#### WPD04

Drillhole WPD04 has the best mineralized intersection: 4.1 m at 2.2% Zn, 0.2% Cu, 0.5% Pb, 0.12 ppm Au and

14 ppm Ag from 97.7 to 101.8 m. This drillhole also intersected 1.55 m at 0.5% Cu, 0.3% Pb, 0.13 ppm Au, 12 ppm Ag from 178.6 to 180.5 m down the hole.

The main zone of mineralization intersected by WPD04 has sections of massive to semimassive sulfides alternating with gneiss containing disseminated sulfides as veinlets and interstitial to silicate minerals. Pyrrhotite is generally the dominant sulfide with lesser pyrite and minor sphalerite, chalcopyrite and galena (Fig. 3a,c). In places, pyrite is dominant and is present as irregular spongy masses with abundant inclusions and as euhedral crystals (Fig. 3e). Galena commonly contains small inclusions of native bismuth (Fig. 3f). The zinc spinel gahnite was commonly observed in association with sphalerite (Fig. 3a–d). Some sulfides appear to have been remobilized post-peak metamorphism and fill fractures in garnet (Fig. 3d) and replace biotite along cleavage (Fig. 4).

Sulfides in the second zone of mineralization consist predominantly of pyrrhotite with minor chalcopyrite, sphalerite, galena and native bismuth. The sulfides are intergrown with clinochlore (a colourless chlorite showing twinning and inclined extinction) and hornblende (Fig. 5a,b), or in places polysynthetically twinned cummingtonite (Fig. 5c).

A conventional lithological log for WPD04 is given in Appendix 3a. A simplified lithological log together with a summary plot of TIR and SWIR mineral group data is included in Figure 6. Both TIR and SWIR summary plots for WPD04 show a clear change in mineral assemblage above and below the main zone of mineralization. This is reflected in the logs and supported by petrography.

The dominant lithology intersected in the hangingwall (i.e. structurally above the main mineralized horizon and overlying the mineralization assuming everything is the right way up) is a fine-grained compositionally layered rock (Fig. 7a). The dark-coloured layers are composed dominantly of hornblende and, in places, also biotite with interstitial plagioclase; whereas, the light-coloured layers are composed predominantly of plagioclase and quartz with minor hornblende (Fig. 7b). The layering may represent original bedding as there is apparent cross-bedding in places (Fig. 7a). More massive amphibolite horizons are interspersed with the compositionally layered rocks. These are composed dominantly of hornblende and plagioclase with minor biotite and quartz (Fig. 8a). In places, the amphibolite is garnet bearing (Fig. 8b). There is a gradation between amphibolite and massive rock composed of biotite, amphibole, feldspar and quartz  $\pm$  garnet that was logged as mafic gneiss (Fig. 8c); more quartz-rich massive rocks were logged as intermediate gneiss.

Coarse-grained pegmatites composed of quartz, plagioclase, orthoclase, white mica and tourmaline intrude the upper part of the sequence (Fig. 9). These show no sign of deformation. They preserve an igneous texture and are thus post-deformation and peak metamorphism, assuming metamorphism coincided with deformation and was not static.

In the footwall (beneath the main mineralized horizon), felsic gneiss is the dominant rock type. The gneiss varies in composition but quartz is the dominant mineral; biotite is generally present and defines the foliation. Although the TIR summary plot (Fig. 6a) shows abundant white mica in the gneisses, muscovite was only observed in gneiss within 7 m of the main zone of mineralization. Elsewhere biotite was the only mica present in the gneiss as correctly shown in the SWIR summary plot (Fig. 6b). Garnet is scattered throughout the gneiss and is abundant in places. The garnet ranges in size from less than 100  $\mu$ m across (Fig. 10a) to several mm across (Fig. 10b), even in the same section, and it varies from subhedral crystals to irregular aggregates. Euhedral to subhedral staurolite crystals are locally concentrated in many of the gneisses (Fig. 10c). Sillimanite was observed in a few sections as irregular elongate crystals (Fig. 10d) and as sheaths of fibrous crystals replacing muscovite in gneiss close to mineralization (Fig. 10e). Kyanite is also present in many of the gneisses (Fig. 10f). Sillimanite and kyanite were differentiated on the basis of the stronger birefringence and straight extinction of the former, and the inclined extinction of the latter.

Fine-grained amphibolite horizons are interspersed with felsic gneiss and some of these contain abundant garnet. Between 200.9 and 215.8 m, the felsic gneiss is intruded by fine- to medium-grained metadolerite which in places has remnant altered plagioclase crystals and rare remnant pyroxene in a groundmass of fine-grained recrystallized hornblende (Fig. 11). The metadolerite is in turn intruded by fine-grained post-metamorphic dolerite.

## WPD07

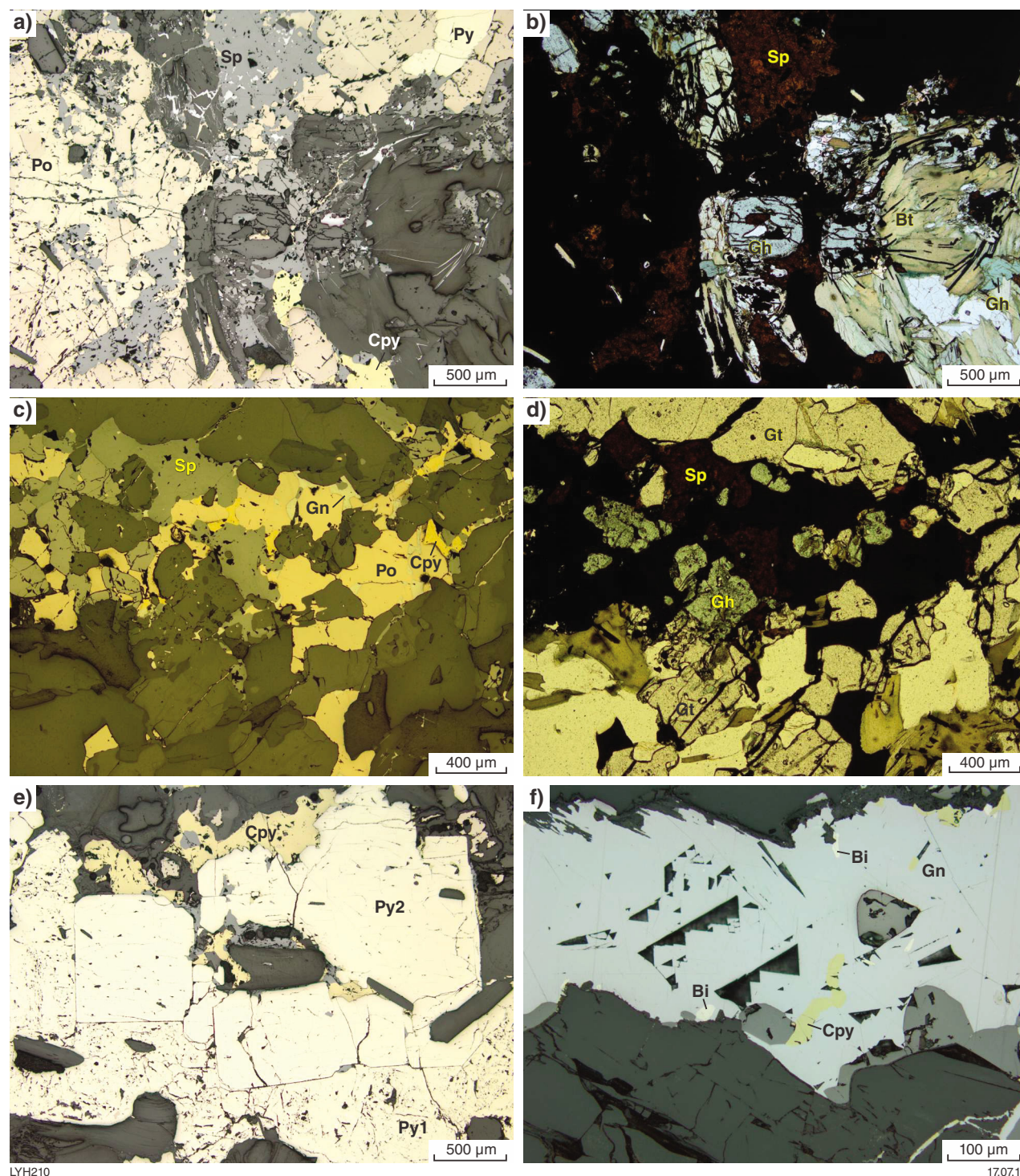
WPD07, drilled 1.37 km east-northeast of WPD04, has the second best intersection of base metal mineralization: 3.05 m at 2.6% Zn, 0.2% Cu and 0.5% Pb from 118.9 – 121.95 m. This drillhole also intersected 1.45 m at 0.85 ppm Au from 163.6 – 165.05 m.

The massive sulfides in WPD07 consist predominantly of recrystallized euhedral to subhedral pyrite with interstitial pyrrhotite, sphalerite, chalcopyrite and galena (Fig. 12). Biotite, chlorite and hornblende are interstitial to the sulfides; silicates also occur along fractures in the pyrite.

The weak gold mineralization at 163.6 – 165.05 m is related to a zone of disseminated sulfides about 5 cm wide adjacent to a 2 cm wide quartz vein within what is possibly a metamorphosed shear zone. The sulfides include arsenopyrite, pyrite and pyrrhotite and are aligned parallel to schistosity defined by biotite (Fig. 13).

A conventional lithological log for WPD07 is given in Appendix 3b. A simplified lithological log together with a summary plot of TIR and SWIR mineral group data is included in Figure 14.





LYH210

17.07.17

**Figure 3.** Main zone of mineralization in WPD04: a) pyrrhotite (Po), pyrite (Py), sphalerite (Sp) and chalcopyrite (Cpy); GSWA 116858, 101.2 m; reflected light; b) same field as a) showing gahnite (Gh) and biotite (Bt); plane-polarized light; c) pyrrhotite, sphalerite, chalcopyrite and galena (Gn); GSWA 116738, 100.0 m; reflected light; d) same field as a) showing gahnite and garnet (Gt); plane-polarized light; e) irregular, inclusion-filled pyrite (Py1) and chalcopyrite interstitial to subhedral, relatively clear pyrite (Py2); GSWA 113736, 98.94 m; reflected light; f) galena with inclusions of native bismuth (Bi) and chalcopyrite; GSWA 116858, 101.2 m; reflected light



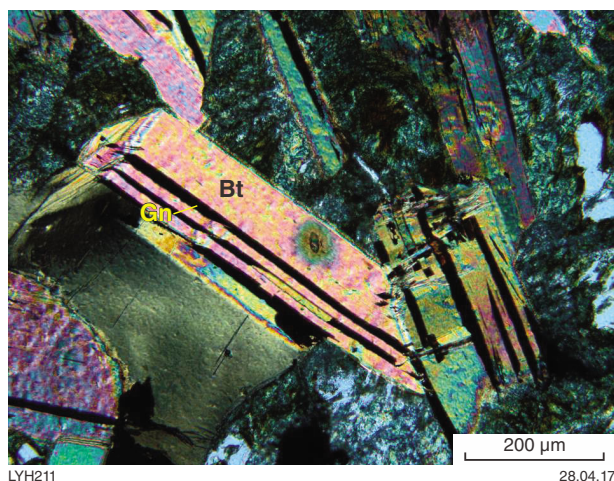


**Figure 4. Galena (Gn) replacing biotite (Bt) along cleavage; GSWA 116736, 98.94 m, WPD04; crossed polars**

The succession intersected in the hangingwall is similar to that intersected above the mineralization in WPD04, in which compositionally layered rock alternates with amphibolite and mafic gneiss. The amphibolite has been intruded by metadolerite at 86.1 – 88.5 m adjacent to a massive quartz vein.

Immediately below the massive sulfide mineralization, there is a zone of disseminated sulfides including pyrite and pyrrhotite with minor chalcopyrite and galena (Fig. 15a). This is hosted within a gneiss composed of quartz, plagioclase, biotite, hornblende, magnetite and ilmenite with large elongate crystals of gedrite parallel to foliation. The gedrite contains numerous inclusions of hornblende, biotite, quartz, plagioclase and oxides and appears to have overgrown and replaced these minerals (Fig. 15b). Beneath this altered zone down to 136.5 m, there is felsic gneiss composed of quartz–biotite ± plagioclase ± garnet ± staurolite ± sillimanite ± kyanite similar to that in WPD04. There is also felsic gneiss intercalated with amphibolite and mafic gneiss from 166.1 to 194.3 m. Between these felsic gneiss intervals, there is an interval of compositionally layered rock with intercalated amphibolite similar to the interval above the mineralization. There has possibly been some structural repetition as the second interval of gneiss is beneath a strongly disrupted schistose rock interpreted as a metamorphosed shear zone.

From 194.3 m to the bottom of the hole at 220.5 m, there is a light-grey massive rock unlike any found in WPD04. It has a granoblastic texture and consists of quartz, microcline, plagioclase, biotite, muscovite and minor tourmaline and opaque minerals (Fig. 16a) and is interpreted to be a recrystallized felsic volcanic rock. In places, it contains what appear to be lighter coloured fragments up to 4 cm across which are compositionally similar to the groundmass except that white mica dominates instead of biotite (Fig. 16b,c). The matrix to the fragments contains significantly more biotite than the more massive rock and also contains more tourmaline (Fig. 16d).

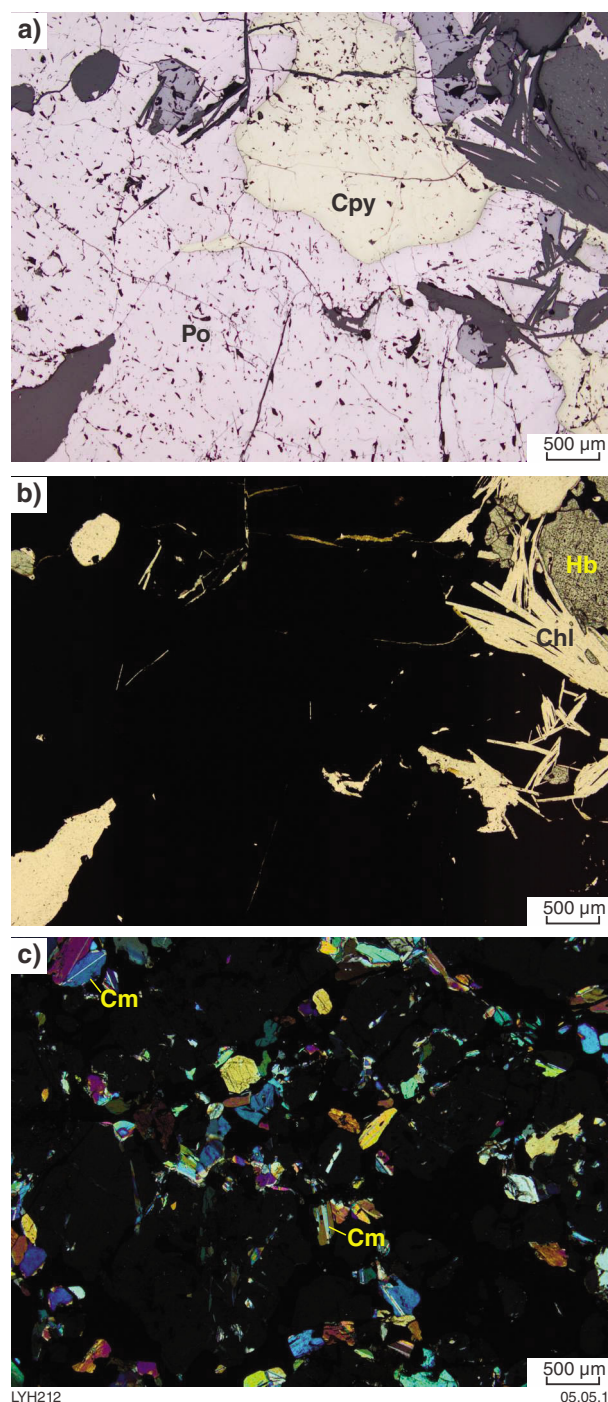


**Figure 5. Second zone of mineralization in WPD04: a) massive pyrrhotite (Po), chalcopyrite (Cpy) and sphalerite (Sp); GSWA 116753, 179.3 m; reflected light; b) same field as a) showing clinocllore (Chl) and hornblende (Hb); plane-polarized light; c) cummingtonite (Cm) interstitial to sulfides; GSWA 206369, 178.8 m; crossed polars**

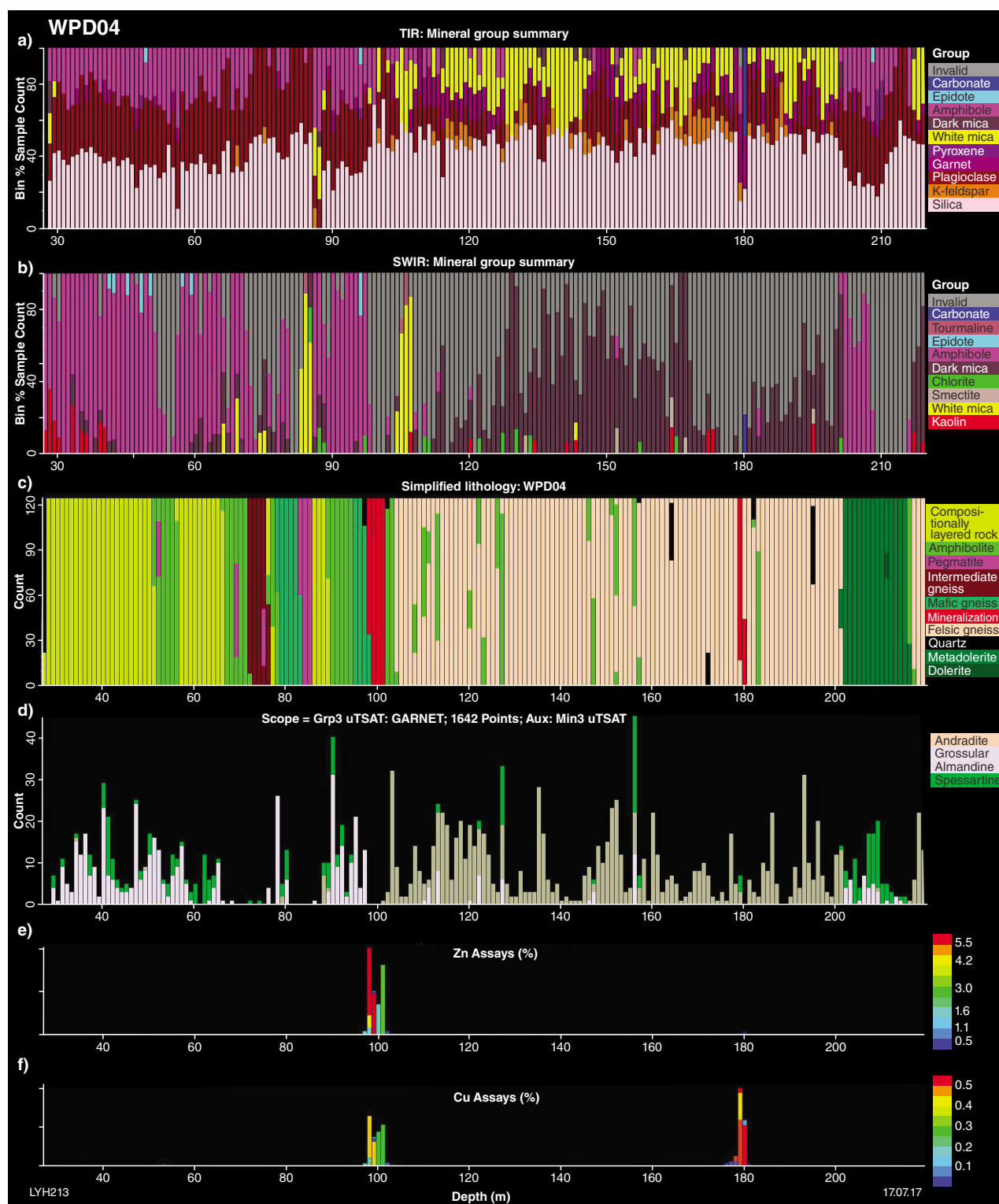
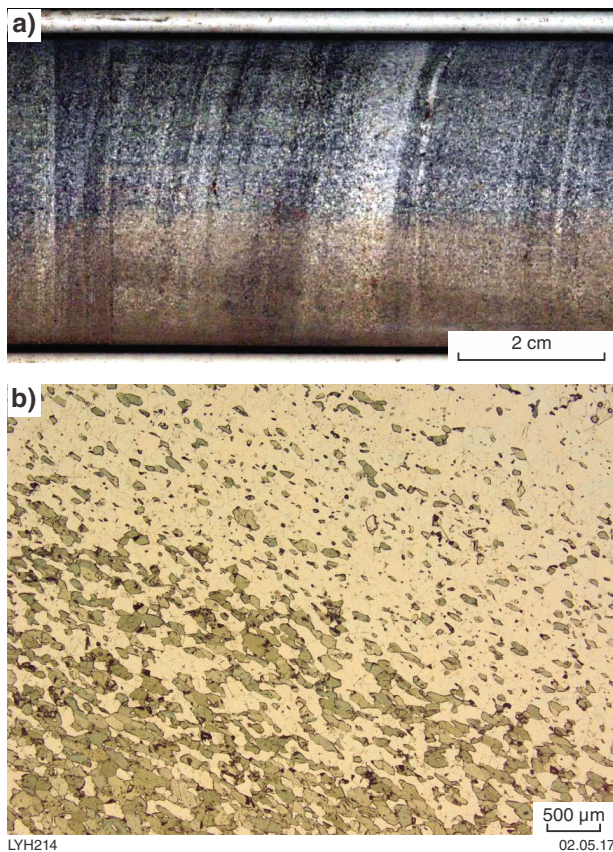
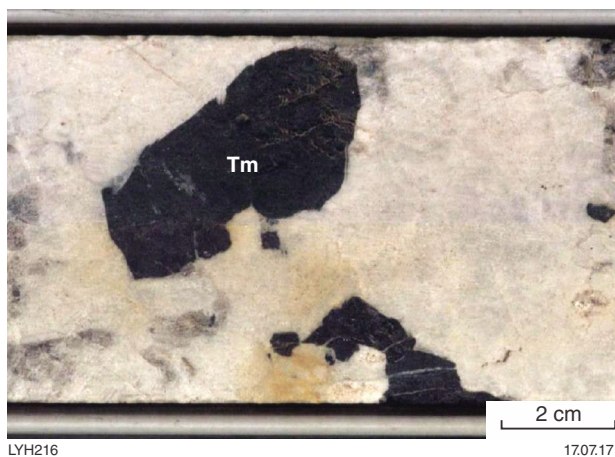


Figure 6. HyLogger, lithology and assay data for WPD04: a) TIR group summary; b) SWIR group summary; c) simplified log; d) downhole distribution of garnets (TIR mineral 3); e) % Zn; f) % Cu





**Figure 7.** Compositionally layered rock: a) core showing alternation of dark hornblende-rich layers and lighter coloured plagioclase and quartz layers; GSWA 116728, 48.3 m WPD04; b) photomicrograph of thin section from core sample in a); hornblende predominates in lower left, and plagioclase and quartz predominate in upper right of section



**Figure 9.** Pegmatite with coarse-grained tourmaline (Tm); 84.55 m, WPD04

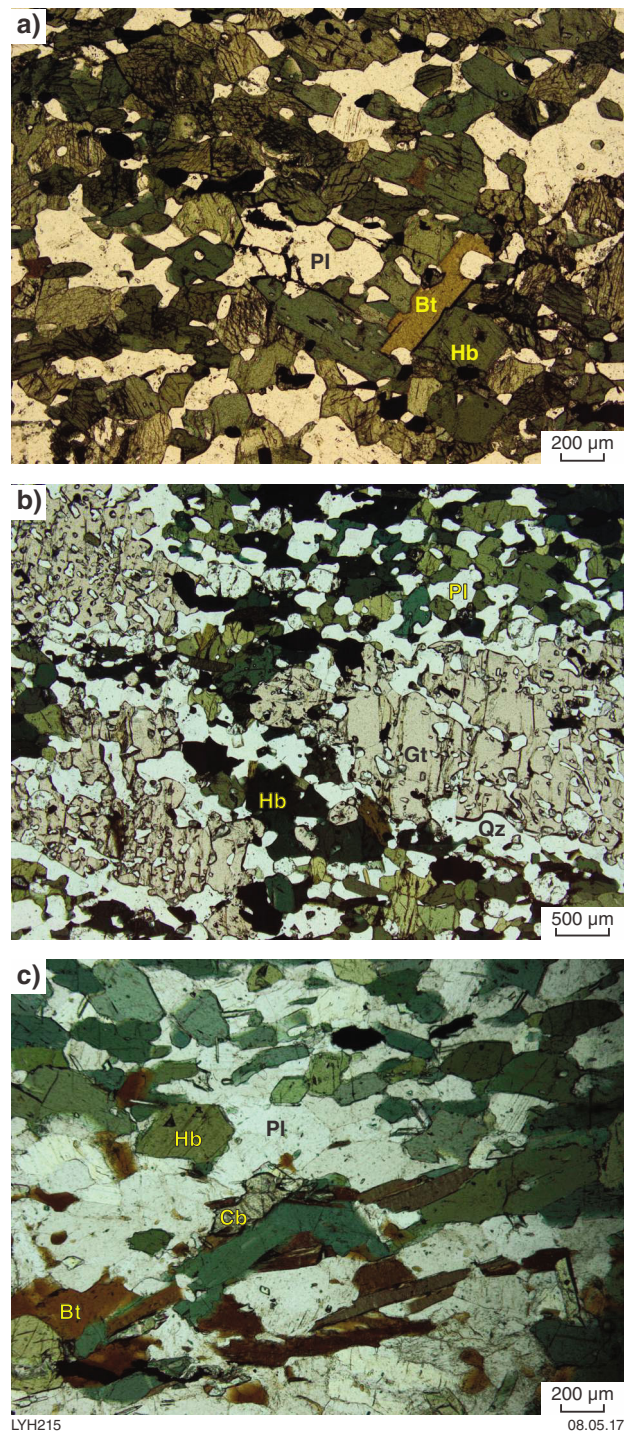


**Figure 8.** Amphibolite and mafic gneiss: a) amphibolite composed of abundant hornblende (Hb), plagioclase (Pl) and minor biotite (Bt); GSWA 116725, 52.1 m, WPD04; plane-polarized light; b) garnet aggregates in amphibolite; GSWA 206352, 55.0 m, WPD04; plane-polarized light; c) mafic gneiss composed of hornblende, biotite, plagioclase, quartz and minor carbonate (Cb); GSWA 206357, 95.7 m, WPD04; plane-polarized light



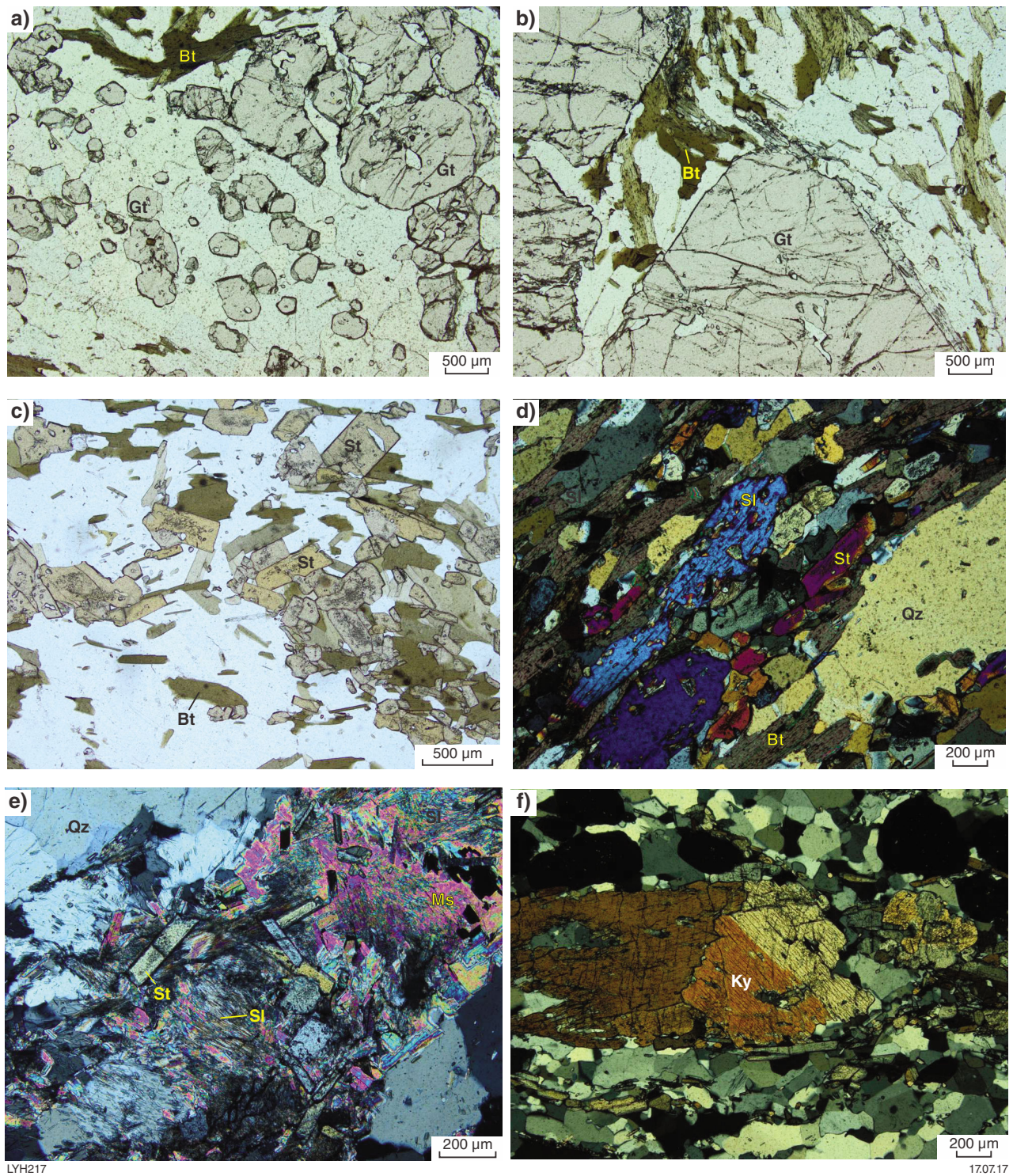


**Figure 10.** Minerals in gneiss beneath mineralization: a) small-to medium-sized anhedral garnets (Gt) and biotite (Bt) in quartz-rich matrix; GSWA 203362, 119.2 m, WPD04; plane-polarized light; b) large subhedral garnets in matrix of quartz and biotite; same section as a); plane-polarized light; c) euhedral to subhedral staurolite (St) in matrix of quartz and biotite; GSWA 116747, 112.4 m, WPD04; plane-polarized light; d) elongate sillimanite (Si), staurolite, biotite and quartz; GSWA 206362, 119.2 m, WPD04; crossed polars; e) fibrous sillimanite replacing muscovite (Ms) and quartz; GSWA 116743, 108 m, WPD04; crossed polars; f) kyanite (Ky); crossed polars



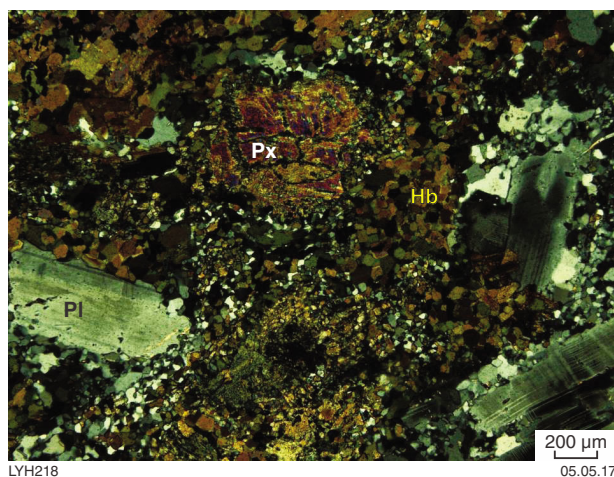


**Figure 11.** Metagabbro with remnant altered plagioclase crystals (Pl) and rare remnant pyroxene (Px) in a groundmass of fine-grained recrystallized hornblende (Hb); GSWA 116754, 211.5 m, WPD04; crossed polars

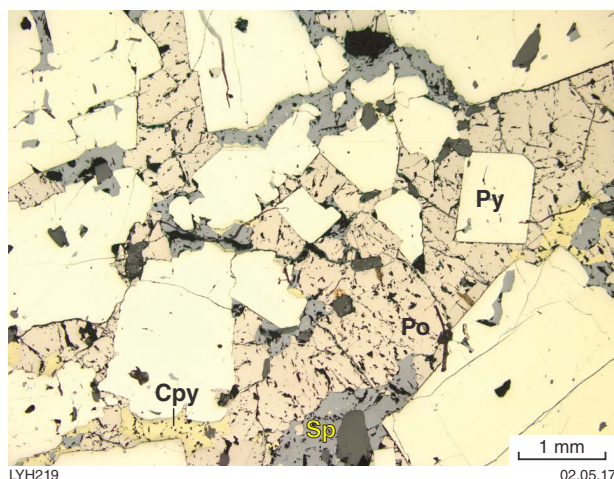


**Figure 12.** Massive sulfide mineralization in WPD07. Euhedral to subhedral pyrite (Py) in matrix of pyrrhotite (Po), sphalerite (Sp) and chalcopyrite (Cpy); GSWA 116763, 118.9 m; reflected light

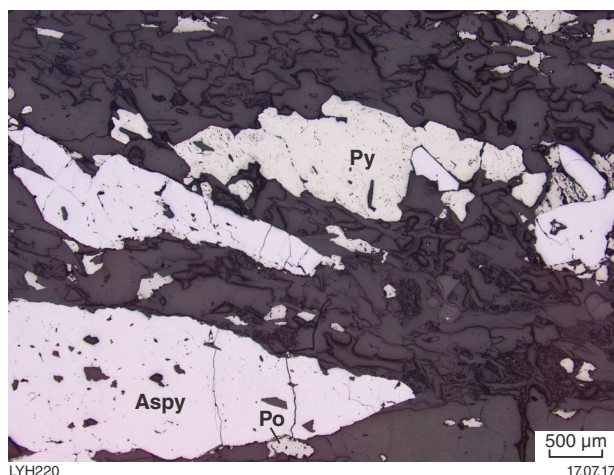


**Figure 13.** Disseminated arsenopyrite (Aspy), pyrite (Py) and pyrrhotite (Po) adjacent to quartz vein in possible shear zone; GSWA 116769, 163.7 m; reflected light

## WPD02

WPD02 intersected a narrow zone of massive sulfides containing 1.79% Zn, 0.3% Cu and 0.2% Pb over 0.5 m between 178.5 and 179.0 m. The sulfides consist predominantly of coarse-grained, subhedral pyrite with minor, interstitial, inclusion-filled pyrite, chalcopyrite and sphalerite (Fig. 17a). Elsewhere, there is interstitial pyrrhotite and magnetite. Galena is present as small inclusions in the subhedral pyrite. Quartz is also interstitial to the pyrite. Gahnite is abundant in places (Fig. 17b) suggesting zinc levels are higher than indicated by the assays (the gahnite may not completely dissolve in a three-acid digest treatment).

A conventional lithological log for WPD02 is given in Appendix 3c. A simplified lithological log together with a summary plot of TIR and SWIR mineral group data is included in Figure 18.

As in WPD04 and WPD07, the upper part of WPD02 consists predominantly of compositionally layered rock with intercalated amphibolite, and mafic and intermediate gneiss. Between 175.4 and 229.2 m, there is predominantly felsic gneiss similar to that observed in WPD04 and WPD07 composed of variable amounts of quartz, plagioclase, biotite, staurolite and kyanite. This includes 2.9 m of gneiss above the massive sulfides containing disseminated gahnite. The gneiss immediately below the massive sulfides also contains disseminated gahnite. Two metres below the massive sulfides there is a 20 cm interval containing abundant tourmaline (Fig. 19a,b). Thin horizons of amphibolite and compositionally layered rock similar to those in the upper part of the drillhole are interlayered with the felsic gneiss. From 229.2 m to the bottom of the drillhole at 237.3 m, there is a light-grey rock consisting of quartz, microcline, plagioclase, biotite, white mica, minor tourmaline and opaque minerals with a fragmental texture in places. This is similar to the rock interpreted to be a metamorphosed felsic volcanic rock at the bottom of the WPD07 drillhole. A compositionally similar rock was also intersected between 194.4 and 195.3 m. A felsic rock with layering defined by variations in grain size and composition occurs at 223.7 m (GSWA 206815). This rock contains andalusite (identified on the basis of low birefringence, parallel extinction and length fast character) and minor tourmaline in a crystalline groundmass of microcline, biotite and quartz (Fig. 20). This is possibly after waterlain tuff on the basis of composition and gradation in grain size that could possibly reflect graded bedding that has survived metamorphism.

The upper part of the core has been intruded by gabbro composed of randomly orientated plagioclase laths with interstitial altered pyroxene and minor oxides (Fig. 21). This gabbro is not foliated and was therefore intruded after deformation. Coarse-grained pegmatite with scattered tourmaline intrudes both the upper and lower parts of the sequence and is also post-peak metamorphism.

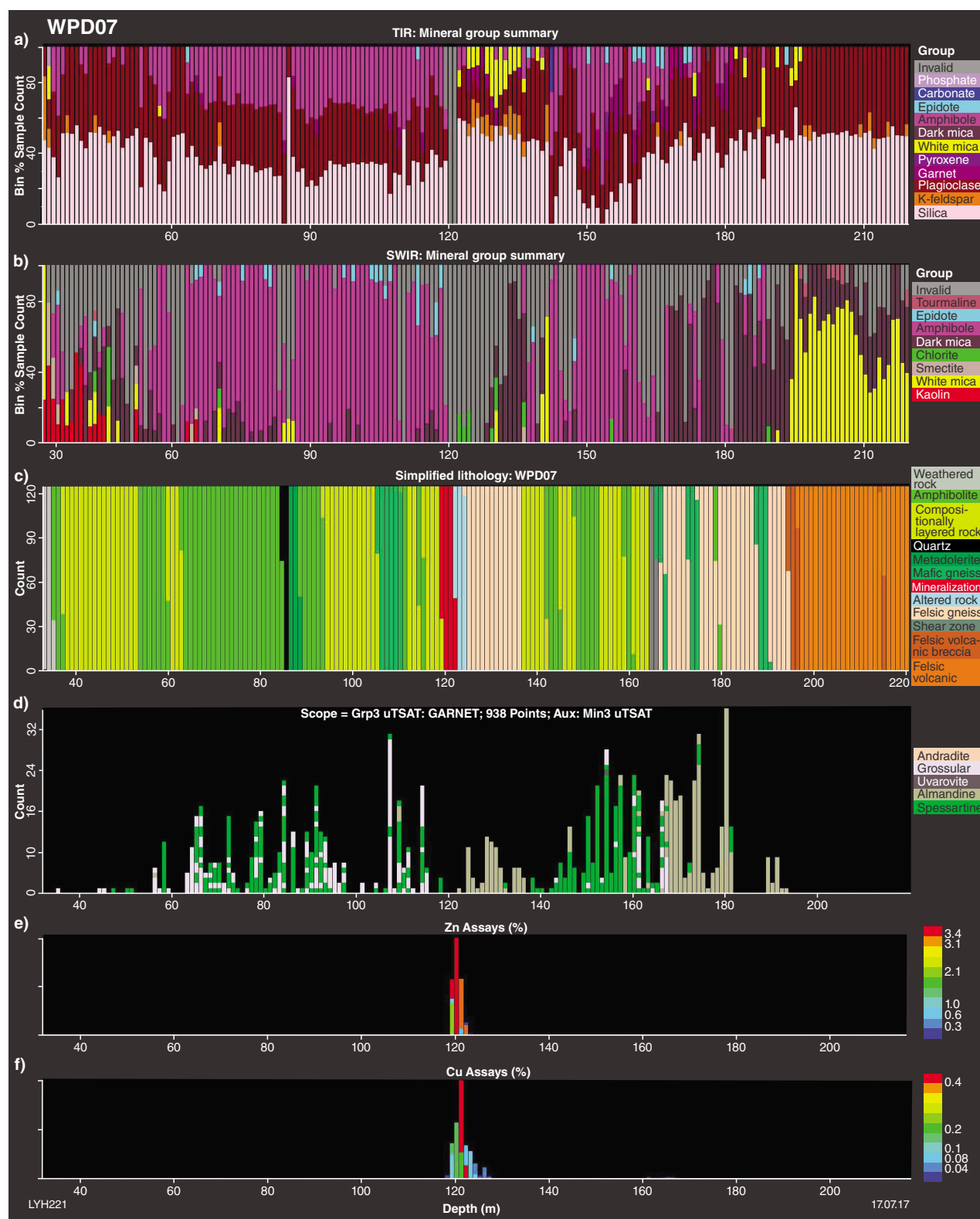
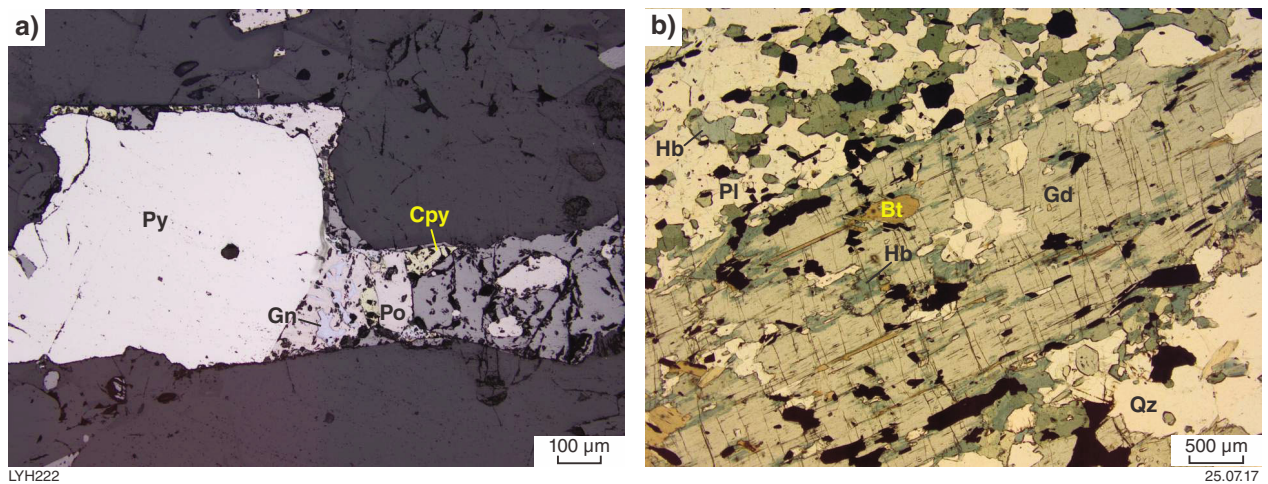
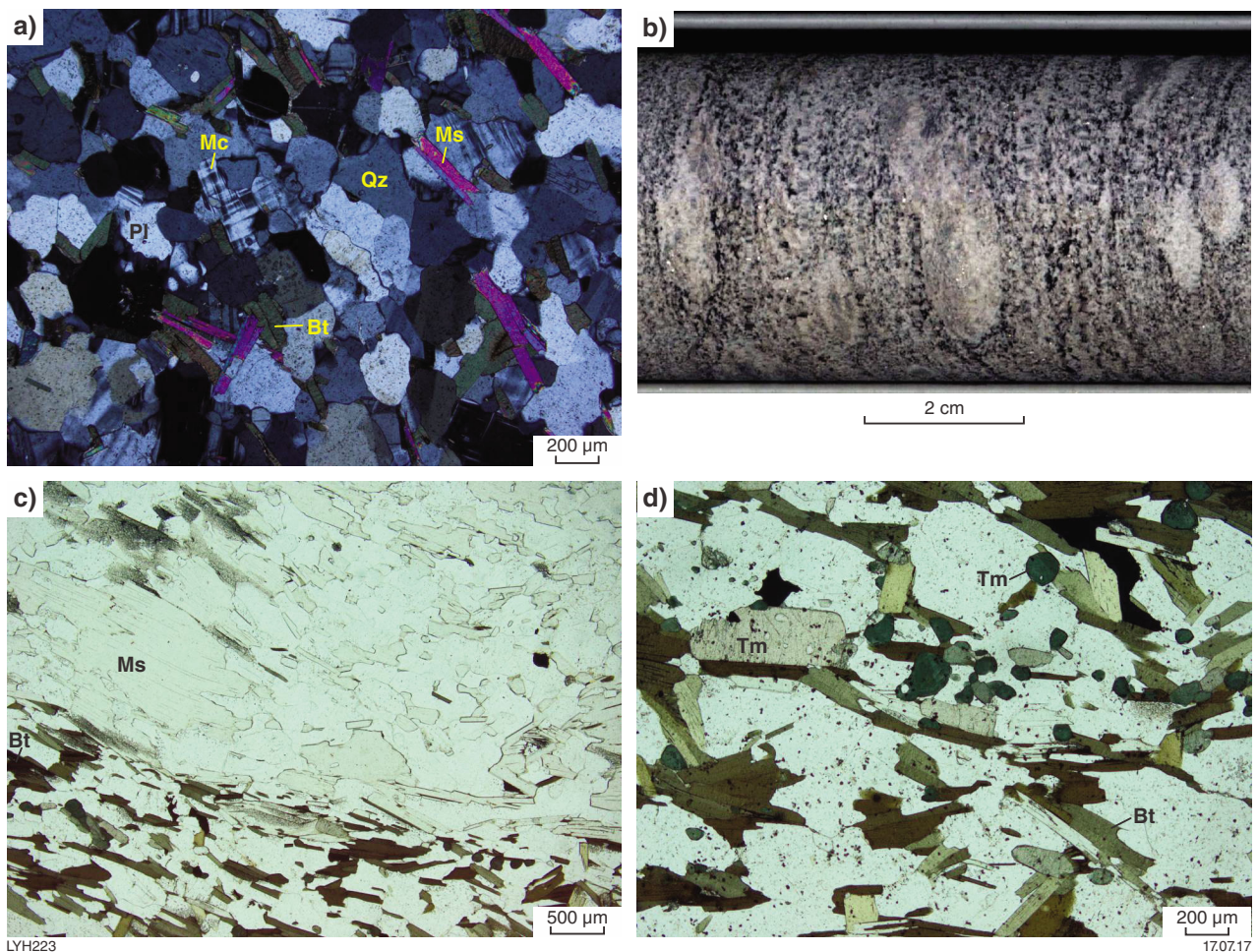


Figure 14. HyLogger, lithology and assay data for WPD07: a) TIR group summary; b) SWIR group summary; c) simplified log; d) downhole distribution of garnets (TIR mineral 3); e) % Zn; f) % Cu





**Figure 15.** Alteration zone beneath mineralization in WPD07: a) disseminated sulfides including pyrite (Py), pyrrhotite (Po), galena (Gn) and chalcopyrite (Cpy); GSWA 116766, 123.0 m; reflected light; b) large elongate crystal of gedrite (Gd) growing at the expense of hornblende (Hb), biotite (Bt), quartz (Qz) and oxides (black); same section as a)



**Figure 16.** Possible felsic volcanic rock and volcanic breccia at the bottom of the WPD07 drillhole: a) massive rock composed dominantly of quartz (Qz), microcline (Mc), plagioclase (Pl), biotite (Bt) and muscovite (Ms); GSWA 116733, 220.4 m; crossed polars; b) core sample showing light coloured fragments in darker matrix; 215.4 m; c) photomicrograph showing boundary between light-coloured fragment and darker matrix. Muscovite is the dominant mica in the fragment and biotite is the dominant mica in the matrix; GSWA 116772, 220.5 m; plane-polarized light; d) abundant tourmaline (Tm) and biotite in matrix to fragments; same section as c)



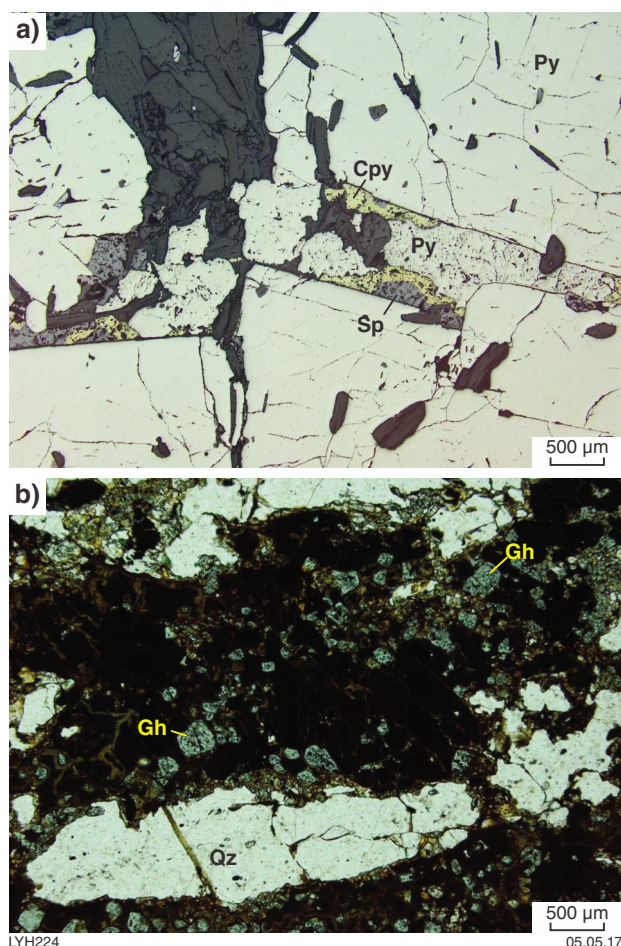


**Figure 17. Mineralization from WPD02: a) coarse-grained subhedral pyrite (Py) with interstitial inclusion-filled pyrite, chalcopyrite (Cpy) and sphalerite (Sp); GSWA 206804, 178.5 m; reflected light; b) abundant gahnite (Gh) associated with sulfides (black) and quartz (Qz); same section as a)**

## WPD13

Diamond drillhole WPD13 intersected a zone of alternating sulfide mineralization and felsic gneiss between 114.15 and 119.62 m. The best base metal intersections are 0.45 m at 1.2% Zn, 0.2% Cu and 0.1 % Pb from 114.5 – 114.6 m, and 0.3 m at 1.1 % Zn, 1.1% Cu and 0.5 % Pb from 117.0 – 117.3 m. Sulfides infill the spaces between quartz (after metachert?) fragments within an interpreted metamorphosed volcanic breccia and also occur as narrow horizons of massive sulfides and as disseminated sulfides in gneiss. Euhedral to subhedral pyrite is the dominant sulfide with interstitial spongy melnikovite pyrite, pyrrhotite and minor chalcopyrite, sphalerite and galena. Gahnite and magnetite are associated with the sulfides in places and also occur in the gneisses interlayered with the sulfides.

A conventional lithological log for WPD013 is given in Appendix 3d. A simplified lithological log together with a summary plot of TIR and SWIR mineral group data is included in Figure 22.

As in the other drillcore described above from the Kingsley Prospect, compositionally layered rocks with intercalated amphibolite and mafic gneiss dominate in the core above the mineralization. The compositionally layered rock has been intruded by dolerite.

Beneath and interlayered with the mineralization, there is felsic gneiss composed of quartz  $\pm$  plagioclase  $\pm$  phlogopite (or biotite)  $\pm$  muscovite  $\pm$  kyanite  $\pm$  staurolite  $\pm$  sillimanite  $\pm$  gahnite  $\pm$  garnet  $\pm$  hornblende  $\pm$  zoisite in the vicinity of mineralization and quartz + biotite  $\pm$  garnet  $\pm$  plagioclase  $\pm$  kyanite  $\pm$  staurolite farther from mineralization. Farther downhole, there is amphibolite and compositionally layered rock similar to that in the upper part of the hole and intermediate gneiss composed of plagioclase, quartz, biotite, hornblende and minor disseminated ilmenite.

## Jack Prospect

### WPD03

Two intervals of low-grade copper mineralization were intersected in this drillhole: 0.7 m at 1.3% Cu from 112.9 – 113.6 m and 0.5 m at 0.63% Cu from 118.1 – 118.6 m. The sulfides infill fractures within a gabbro. Pyrrhotite is the dominant sulfide but chalcopyrite is locally abundant (Fig. 23a) and there are traces of pentlandite and cubanite as inclusions within the pyrrhotite (Fig. 23b) and rare flakes of molybdenite (Fig. 23c).

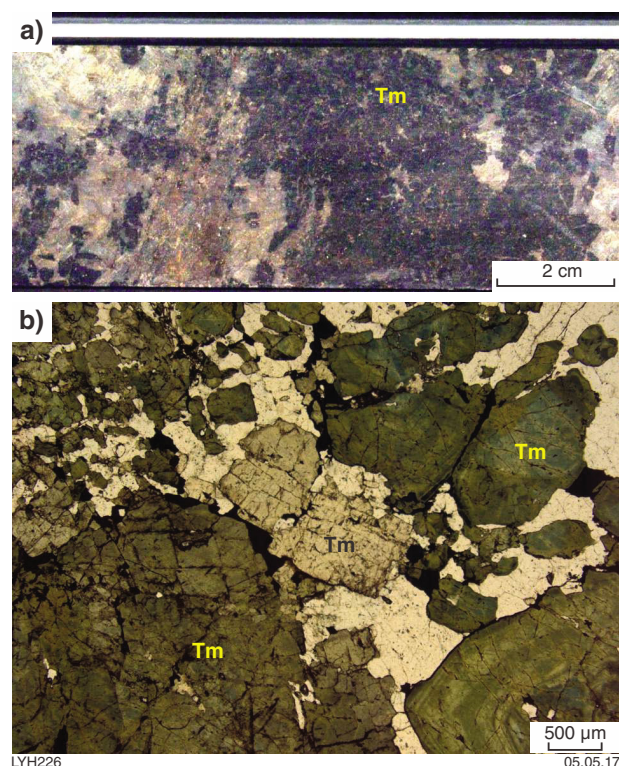
A conventional lithological log for WPD03 is given in Appendix 3e. A simplified lithological log together with a summary plot of TIR and SWIR mineral group data is included in Figure 24.

Amphibolite with compositional layering similar to that intersected in the Kingsley drillholes was intersected between 39 and 67.5 m in WPD03. At 67.5 m, there is an intrusive contact with gabbro (Fig. 25a). Gabbro is the dominant rock type in the remainder of the drillhole although there is some intercalated amphibolite. In places, the gabbro is plagioclase rich and grades into anorthosite (Fig. 25b). The HyLogger shows that the plagioclase composition of the anorthosite varies from labradorite to anorthite. There is a sharp contact between gabbro and mafic gneiss with abundant garnets in a matrix of hornblende, plagioclase and quartz at 177.4 m near the bottom of the drillhole. Gneiss with coarse-grained garnets that have haloes of white quartz in a matrix of fine-grained quartz, plagioclase and biotite in the interval 144.8 – 146.4 m is interpreted to be a xenolith within the gabbro.

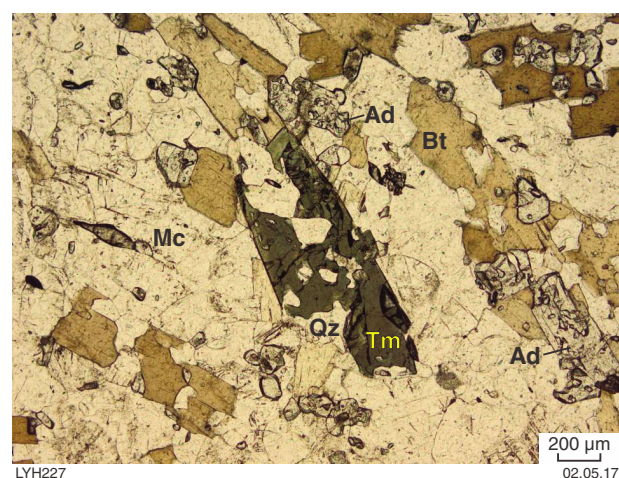


Figure 18. HyLogger, lithology and assay data for WPD02: a) TIR group summary; b) SWIR group summary; c) simplified log; d) downhole distribution of garnets (TIR mineral 3); e) % Zn; f) % Cu





**Figure 19.** Tourmaline-rich (Tm) horizon below mineralization in WPD02: a) core; b) photomicrograph; GSWA 206805B, 182.35 m; plane-polarized light



**Figure 20.** Felsic rock containing andalusite (Ad) and minor tourmaline (Tm) in a crystalline groundmass of microcline (Mc), biotite (Bt) and quartz (Qz); GSWA 206815, 223.7 m, WPD02; plane-polarized light

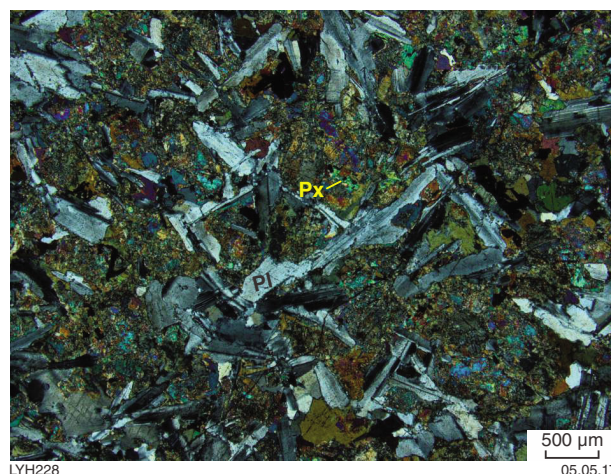


**Figure 21.** Gabbro with randomly orientated plagioclase crystals and partially altered interstitial pyroxene (Px); GSWA 206393, 108.1 m, WPD02; plane-polarized light

## Chemistry of the host succession

Major element and trace element geochemical data for amphibolite and other rock types from Wheatley are given in Table 3.

On the Zr/Ti vs Nb/Y volcanic discrimination diagram of Pearce (1996), most of the rocks logged as amphibolite plot in the basalt field or close to the boundary between basalt and andesite–basaltic andesite (Fig. 26). The two exceptions that plot in the upper part of the andesite–basaltic andesite field are garnet-bearing amphibolites. There is no significant difference on this diagram between the amphibolites from above mineralization at the Kingsley Prospect and those below mineralization. The amphibolite from the Jack Prospect lies in the basalt field to the left of the amphibolites from the Kingsley Prospect and is similar to the gabbro from the Jack Prospect. The amphibolites from the Kingsley Prospect are more similar to the metadolerite from the Kingsley Prospect.

Two samples logged as metafelsic volcanic rock (GSWA 206818) and metafelsic volcanic breccia (GSWA 116772) plot in the rhyodacite–dacite field and andesite field of Winchester and Floyd (1977), respectively (Fig. 27). The breccia contains relatively high Ti (0.72% TiO<sub>2</sub>) and may have a more mafic component in the matrix as suggested by the abundance of biotite. Surprisingly, rocks logged as felsic gneiss plotted in a range of fields from andesite to rhyodacite–dacite to trachyandesite on the volcanic rock classification of Winchester and Floyd (1977), whereas two rocks logged as intermediate gneiss plotted as rhyodacite–dacite and rhyolite, but this may not be meaningful if the rocks had a significant clastic component. The sample plotting as rhyolite (GSWA 206389) contained 73.0% SiO<sub>2</sub> and consisted of aggregates of garnet in a matrix of quartz, plagioclase and biotite; the other sample logged as intermediate gneiss contained 64.1% SiO<sub>2</sub>.

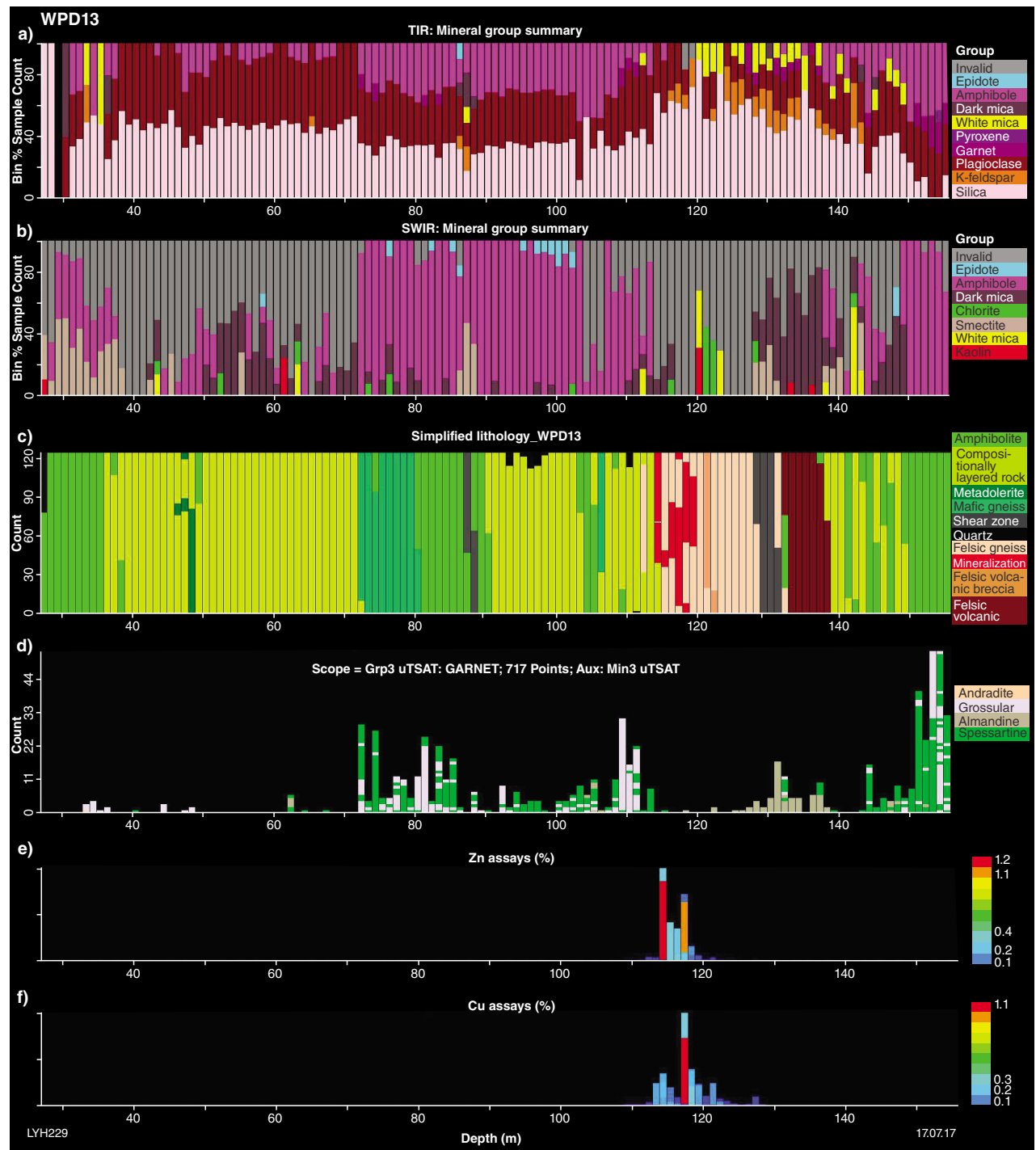
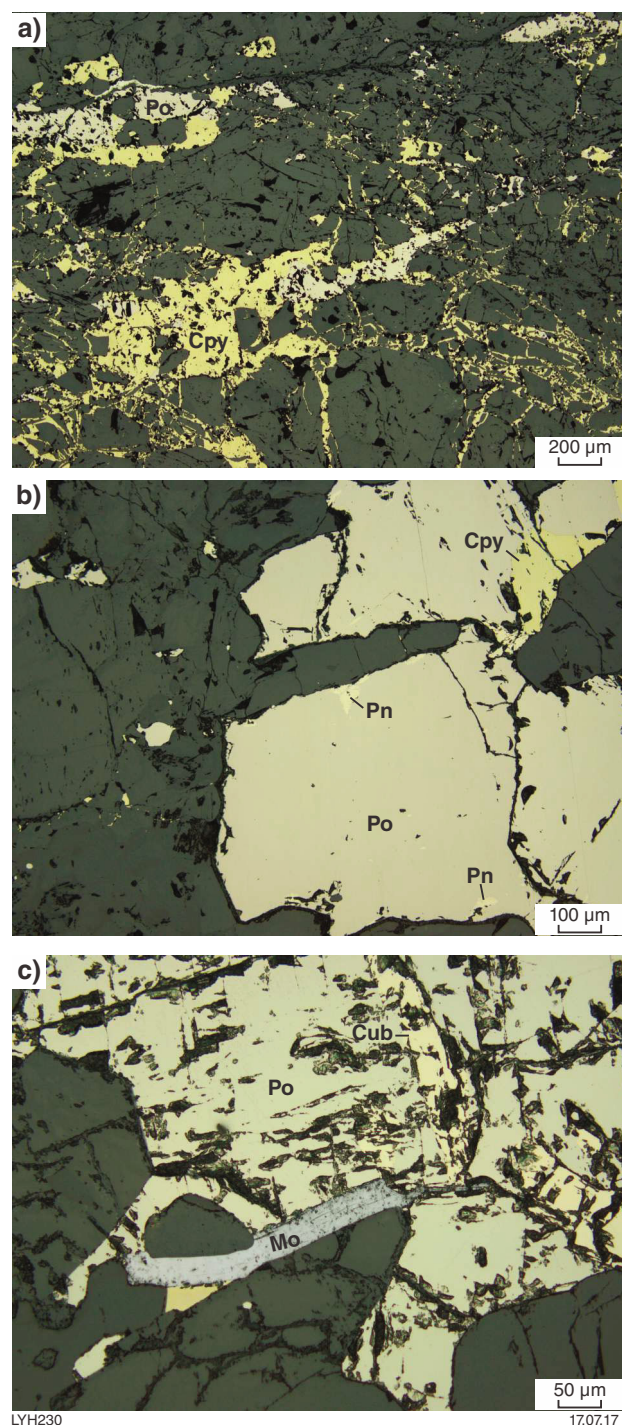


Figure 22. HyLogger, lithology and assay data for WPD13: a) TIR group summary; b) SWIR group summary; c) simplified log; d) downhole distribution of garnets (TIR mineral 3); e) % Zn; f) % Cu





**Figure 23.** Mineralization infilling fractures in gabbro WPD03 at the Jack Prospect: a) chalcopyrite (Cpy) and pyrrhotite (Po); GSWA 204714, 118.1 m; reflected light; b) pyrrhotite with inclusions of pentlandite (Pn) and chalcopyrite; same section as above; reflected light; c) molybdenite (Mo) and cubanite (Cub) associated with pyrrhotite; GSWA 204711, 112.9 m; reflected light

Primitive mantle-normalized plots of the immobile elements for the different rock types at Wheatley are given in Figure 28. The normalization values and order of incompatibility during mantle melting are from Sun and McDonough (1989).

In the case of the amphibolites above mineralization at the Kingsley Prospect (upper amphibolites, Fig. 28a), two different patterns are discernible on the mantle-normalized plot. Three samples (GSWA 206388, 206843 and 206844) have a very flat pattern although enriched relative to primitive mantle. The other four samples (GSWA 224773, 224792, 206392 and 224794) are strongly enriched in Th and light REE, and have negative Nb anomalies. The two garnet-bearing amphibolites (GSWA 224773 and 224792) also have negative Ti anomalies. The amphibolite samples from below the mineralization at Kingsley (lower amphibolites, Fig. 28b), are similar to GSWA 206392 and 224794 from above the mineralization, i.e. they are enriched in Th and have negative Nb anomalies. The amphibolite sample from the Jack Prospect (Fig. 28c), is close to primitive mantle in its incompatible element composition but has slight enrichment in Th and Eu and depletion in Nb and Zr; its HFSE concentrations and ratios are very close to N-MORB.

Samples logged as felsic gneiss below mineralization at the Kingsley Prospect are all strongly enriched in the most incompatible elements although there is a negative Nb anomaly (Fig. 28d). GSWA 224790, 224771 and 224769 have a fairly flat trend for the less incompatible elements and have a negative Ti anomaly, whereas GSWA 224777, 224796, 224781, 224366 and 224779 have a fairly steep trend in the moderate to heavy REE (Fig. 28d).

Intermediate gneiss samples (GSWA 206389 and 224793) from above mineralization at the Kingsley Prospect are strongly enriched in incompatible elements, especially the least compatible elements, but have negative Nb and Ti anomalies (Fig. 28e) and have a similar pattern to GSWA 224790, 224771 and 224769 logged as felsic gneiss.

Samples interpreted as felsic volcanic rock (GSWA 206818) and as felsic volcanic breccia (GSWA 116772) showed very strong enrichment in the least compatible elements but with negative Nb and Ti anomalies (Fig. 28f).

Metadolerite intruding the felsic gneiss in WPD04 (GSWA 224364 and 224365) has a fairly flat to very weakly enriched trend with higher levels of incompatible elements than primitive mantle. However, gabbro intruding amphibolite at the Jack Prospect (GSWA 224776) has similar incompatible chemistry to primitive mantle with minor elevation in Eu and La, and depletion in Nb, Sm and Gd (Fig. 28g).



Figure 24. HyLogger, lithology and assay data for WPD03: a) TIR group summary; b) SWIR group summary; c) simplified log; d) downhole distribution of garnets (TIR mineral 3); e) % Cu

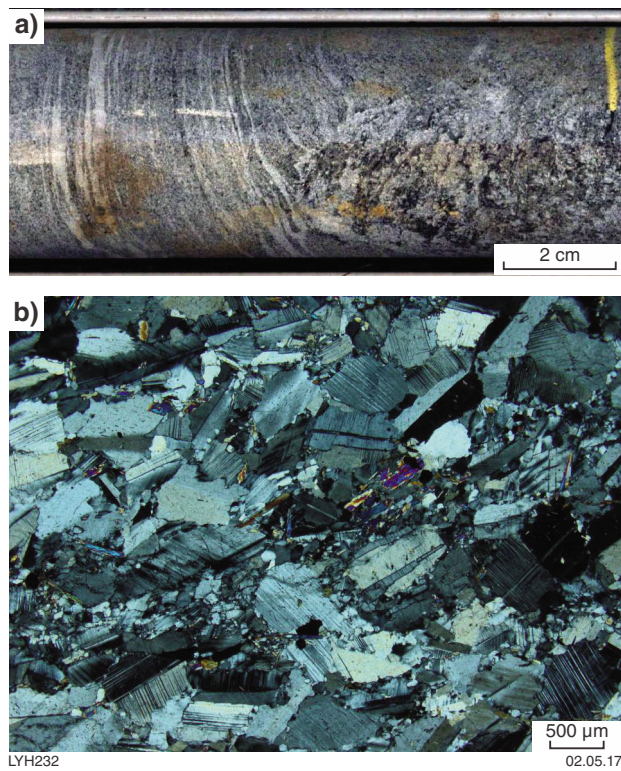


Figure 25. (left) Layered mafic intrusion in WPD03: a) irregular contact between gabbro and amphibolite (68.0 m); b) anorthosite; GSWA 206836, 163.5 m; crossed polars

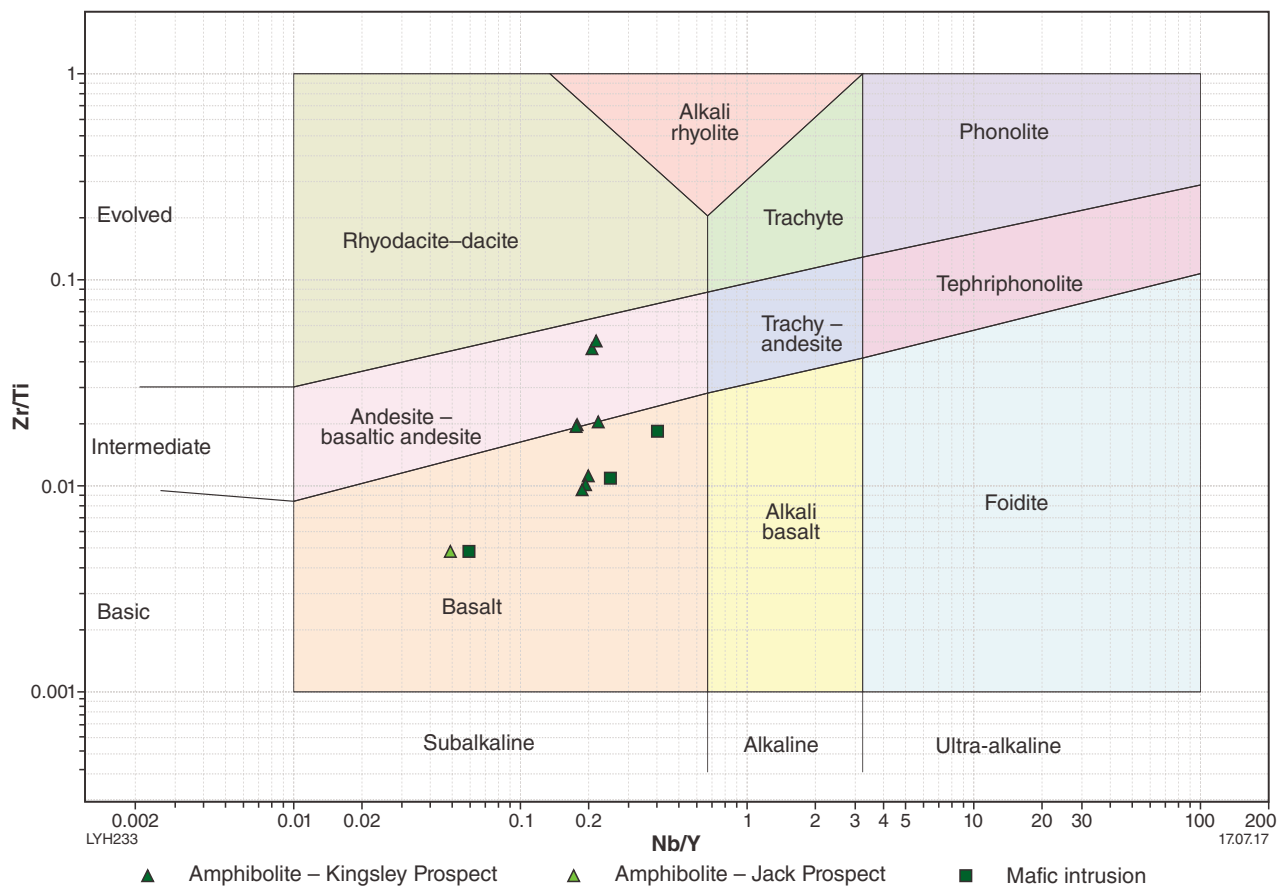
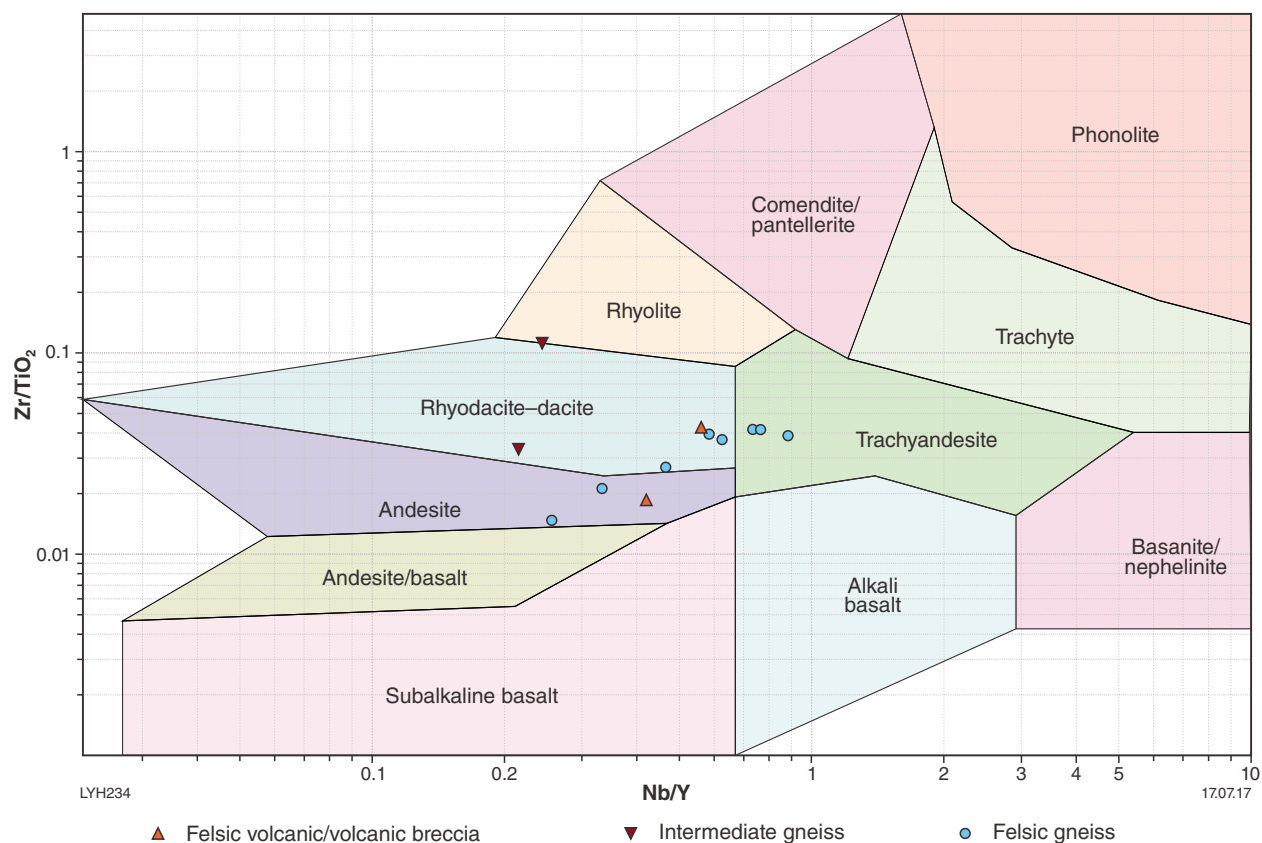


Figure 26. Amphibolites and mafic intrusions plotted on the volcanic discrimination diagram of Pearce (1996)





**Figure 27. Interpreted felsic volcanic rocks and volcanic breccia, intermediate gneiss and rocks logged as felsic gneiss plotted on the volcanic classification diagram of Winchester and Floyd (1977)**

## Mineral distribution and chemistry

### Garnet

Preliminary HyLogger data suggested there was significant spessartine in the rocks above mineralization. As spessartine can form from Mn-rich carbonate and clay or Mn-oxyhydroxides in exhalites overlying VMS deposits (Slack, 2012), the variation in garnet abundance and composition was initially studied using the HyLogger data utilizing the TSG (v7.1.0.049) program. For drillhole WPD04, garnet is significantly more abundant below mineralization than above mineralization (see plots of garnet as first, second and third most abundant minerals; Fig. 29b,c,d). The data also suggested there is a significant difference in composition of the garnet above and below mineralization. Pyrope and almandine dominate in the gneiss below mineralization, and grossular and spessartine dominate above mineralization, although these minerals are also present in some of the mafic rocks below mineralization (most obvious in the plot of the third most abundant mineral, Fig. 29d). The current version of TSG (v. 7.1.0.062) does not have pyrope as a standard but the plot of garnet as the third most abundant mineral (Figs 6d, 29e) also suggests a significant difference in

garnet composition with almandine dominating below mineralization, and grossular and spessartine above mineralization. Similarly, current HyLogger data for the other drillholes (WPD07, WPD02 and WPD13) from the Kingsley Prospect all suggest that almandine dominates in the gneiss below mineralization, and grossular and spessartine dominate in the amphibolites and compositionally layered rocks above mineralization as well as in the mafic horizons below mineralization (Figs 7d, 18d, 22d). Garnet was much less abundant in WPD03 from the Jack Prospect with the HyLogger showing grossular and spessartine as the dominant garnet, except for garnet in an interpreted gneiss xenolith where the HyLogger showed almandine (Fig. 24d).

To test if there was a real difference in composition of garnet above and below mineralization and in different lithologies at Kingsley, garnet in three polished thin sections was analysed by electron microprobe analysis and in 14 sections by SEM; garnet in one section was analysed by both techniques. Where the garnets in the section had different morphology (e.g. anhedral garnet aggregates and euhedral garnet crystals or large and small crystals) each type was analysed. Large garnet crystals were analysed near the centre and near the rim. In sections taken at the boundary of two different lithologies, garnet from both lithologies was analysed.



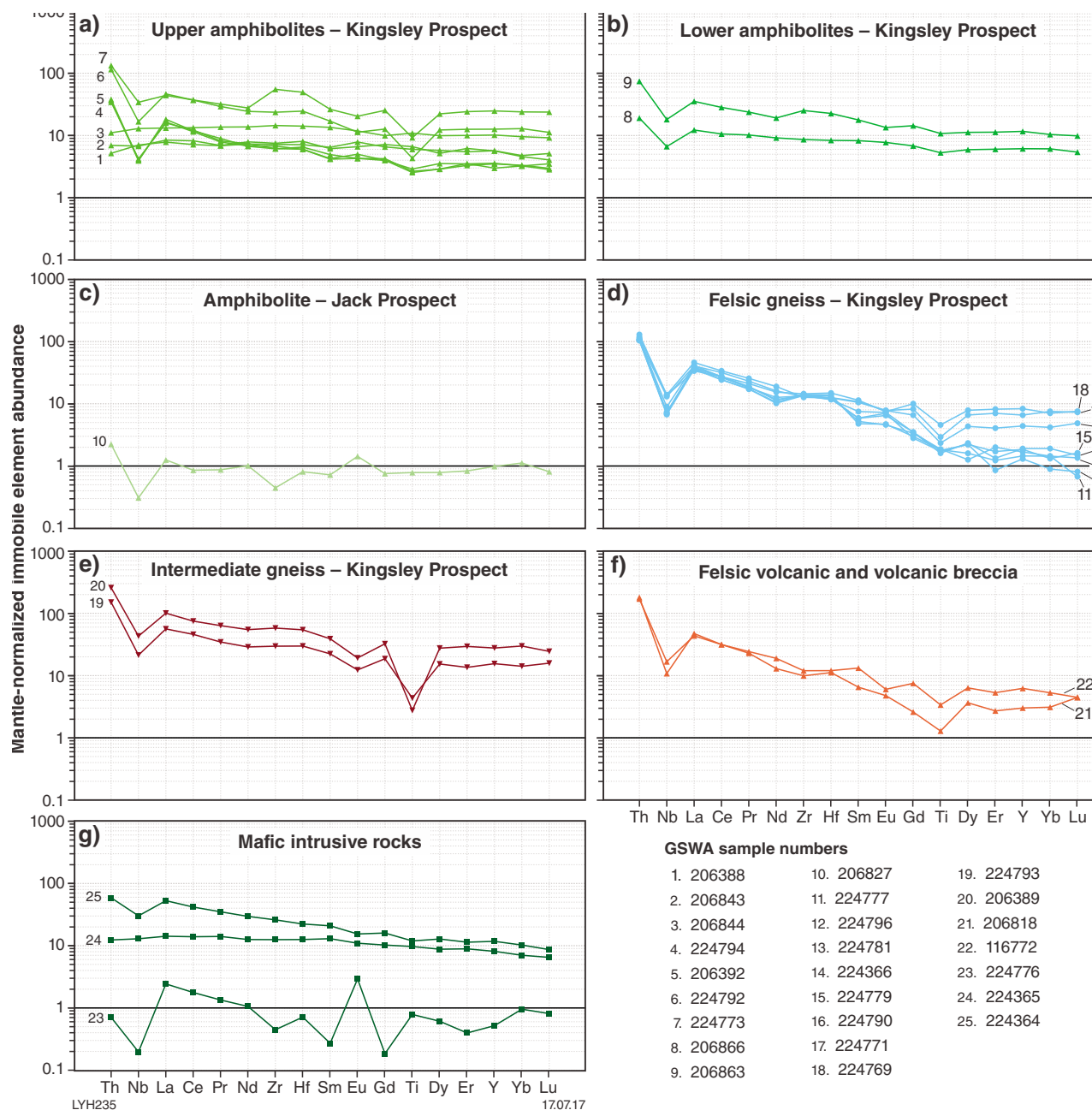


**Figure 28.** Mantle-normalized immobile element abundances for various rock types from Wheatley: a) upper amphibolites, Kingsley Prospect; b) lower amphibolites, Kingsley Prospect; c) amphibolite, Jack Prospect; d) felsic gneiss, Kingsley Prospect; e) intermediate gneiss, Kingsley Prospect; f) ?felsic volcanic rock and volcanic breccia; g) mafic intrusive rocks



**Figure 29.** HyLogger interpretations of variation in garnet composition downhole vs simplified log for WPD04: a) simplified log; b) garnet as mineral 1, TSG v7.1.0.049; c) garnet as mineral 2, TSG v7.1.0.049; d) garnet as mineral 3, TSG v7.1.0.049; e) garnet as mineral 3, TSG v7.1.0.062

The garnet end-member compositions were calculated using the garnet end-member calculator of Andy Tindle ([www.open.ac.uk/earth-research/tindle/AGTWebPages/AGTSoft.html](http://www.open.ac.uk/earth-research/tindle/AGTWebPages/AGTSoft.html), accessed 29 December 2014). Full results are listed in Appendix 4 and 5 respectively and the average results are summarized in Table 4.

SEM analysis of garnet in GSWA 206362 gave slightly higher FeO and SiO<sub>2</sub> and lower MgO and Al<sub>2</sub>O<sub>3</sub> values than analysis by electron microprobe analysis although the differences were small compared with overall differences in composition of the garnets. Where there were several different garnet morphologies in a section, there were generally only minor differences in composition between them for the same lithology (with the exception of GSWA 20677). For those sections taken at the contact of two different lithologies, the garnet composition varied in some cases from one lithology to the next so averages for each lithology are shown in Table 4.

Most of the garnet contained almandine as the most abundant end-member component but the average composition of samples ranges from 45.4% almandine to 80.9% almandine (23.1 – 38.7% Fe). The garnet closest in composition to pure almandine was from the gneiss beneath mineralization, in agreement with the HyLogger data. Pyrope is the next most abundant component in this garnet. Some amphibolite samples from above mineralization also contain garnet with a high almandine composition (up to 72.7%) but in these samples, grossular is the next most abundant component and spessartine is also a significant component. Garnet in one amphibolite sample (GSWA 206354) from above mineralization averages only 52.1% almandine; the remainder is made up of grossular (26.1%), spessartine (9.2%), pyrope (8.8%) and andradite (3.7%). Garnet in the adjacent, lighter coloured compositionally layered rock is similar in composition. Garnet in a sample of amphibolite (GSWA 206377) from 35.5 m below mineralization in WPD07 had the lowest average almandine content of 45.4% (Table 4). One analysis (GSWA 206377a2; Appendix 5) of an inclusion-rich garnet in this sample technically classifies as grossular, based on its calculated grossular (44.5%) vs almandine (39.0%) components. An inclusion-free garnet from the same section (GSWA 206377b2; Appendix 5) contained 37.5 – 38.0% grossular and an aggregate of garnet intergrown with hornblende (GSWA 206377b1; Appendix 5) contained 31.1 – 33.5% grossular. The HyLogger identified the garnets in GSWA 206377 as spessartine but the maximum spessartine content measured in this sample was 6.9% (3.0% Mn). Garnet from a zone of disseminated mineralization (GSWA 116738) within the main mineralized horizon in WPD04 contains the most spessartine molecule, 22.5% (9.7% Mn), but there is no systematic variation in the spessartine content with distance from mineralization. The amphibolites above and below mineralization generally contain more spessartine than the gneisses.

## Gahnite

The HyLogger was incapable of detecting gahnite when it is present at relatively low contents. Petrological examination showed gahnite to be present close to the main mineralized horizon and the lower mineralized horizon in WPD04, and close to mineralization in WPD02 and WPD13, always in association with sulfides. Several grains of gahnite from GSWA 206370 (from 180.6 m in WPD04) were analysed by electron microprobe analysis. The gahnite averaged 33.5 % ZnO, 55.2% Al<sub>2</sub>O<sub>3</sub>, 8.9% Fe, 2.1% MgO, 0.26 % Cr<sub>2</sub>O<sub>3</sub> and 0.04% SiO<sub>2</sub>.

## Staurolite

Staurolite is not included in the standards within TSG but a match can be made down the hole with the SWIR spectra of staurolite from the United States Geological Survey (USGS) spectral library and with the TIR spectra from the John Hopkins University (JHU) spectral library. These are shown against the simplified lithological log for WPD04 in Figure 30. Both show staurolite as being concentrated in the felsic gneiss but the SWIR match shows that staurolite is much more abundant than indicated by the TIR match, and may be influenced by the presence of other minerals such as biotite. Examination of thin sections showed staurolite to be present in small quantities in most felsic gneiss samples, and locally abundant in places (Fig. 10c).

Staurolite crystals in gneiss GSWA 206362 were analysed both by electron microprobe analysis and SEM. Staurolite crystals in two additional gneiss samples were also analysed by SEM. The full results are given in Appendix 6 and a summary of the average compositions for each sample is given in Table 5. Not surprisingly, the electron microprobe results were more reproducible but there was reasonable agreement between the two methods. The slightly higher values given by SEM are due to the fact that the results were totalled to 100% and the hydroxyl ions were not taken into account. Small amounts of Zn<sup>2+</sup> (up to 0.48% ZnO) are replacing Fe<sup>2+</sup> in these samples.

## Kyanite

Although the USGS spectral library gives a SWIR spectrum for kyanite, the spectrum is probably a result of alteration of the kyanite to muscovite because the spectrum is similar to that for muscovite and kyanite does not appear to have a characteristic absorption spectrum. The HyLogger could thus not accurately show the downhole distribution of kyanite. Petrological examination showed kyanite to be sporadically distributed throughout the gneiss beneath the main zone of mineralization at the Kingsley Prospect (Fig. 10f). Kyanite was identified on the basis of its high relief, moderate birefringence (up to first order orange or red), inclined extinction and the presence of twinning (Fig. 10f).

Table 4. Electron microprobe and SEM analyses of garnet from Wheatley

Sample	206352	206354a	206354d	116738	206358	206360a	206360c	206362	206362
Drillhole	WPD04	WPD04	WPD04	WPD04	WPD04	WPD04	WPD04	WPD04	WPD04
Depth	55.0	66.2	66.2	100.0	102.8	108.0	108.0	119.2	119.2
Distance from mineralization (m)	43.4	28.5	28.5	0.0	-1.0	-6.2	-6.2	-17.4	-17.4
Lithology	Amphibolite	Amphibolite	Compositionally layered rock	Disseminated mineralization	Gneiss	Amphibolite	Gneiss	Gneiss	Gneiss
Method	Probe	SEM	SEM	SEM	SEM	SEM	SEM	Probe	SEM
SiO <sub>2</sub>	37.05	39.0	38.7	38.5	39.4	37.1	40.5	37.88	38.9
TiO <sub>2</sub>	0.04	0.0	0.0	0.0	0.0	0.0	0.0	0.02	0.0
Al <sub>2</sub> O <sub>3</sub>	19.96	20.1	19.6	21.3	20.4	20.3	21.0	20.91	19.4
FeO	32.64	24.5	25.3	21.8	30.6	30.4	29.8	33.93	35.1
MnO	3.05	4.0	3.6	9.7	1.2	1.9	1.6	0.47	0.0
MgO	1.25	2.2	1.7	3.9	5.1	2.8	3.4	5.08	4.3
CaO	5.67	10.2	10.8	3.3	3.0	6.6	3.7	2.08	2.3
Na <sub>2</sub> O	0.03	0.0	0.0	0.0	0.4	0.0	0.0	0.03	0.0
K <sub>2</sub> O	0.00	0.0	0.0	0.0	0.2	0.0	0.0	0.01	0.0
ZnO	0.01	0.0	0.1	0.4	0.1	0.0	0.1	0.02	0.0
Cr <sub>2</sub> O <sub>3</sub>	0.01	0.0	0.0	0.0	0.0	0.0	0.0	0.01	0.0
SO <sub>3</sub>	0.00	0.0	0.0	1.1	0.0	0.9	0.0	0.00	0.0
TOTAL	99.71	100.0	100.0	100.0	100.4	100.0	100.0	100.4	100.0
Almandine	71.13	52.1	52.5	52.0	67.8	64.9	71.7	72.97	74.9
Andradite	3.11	3.7	4.7	0.0	2.1	3.7	0.0	2.06	4.0
Grossular	13.54	26.1	27.2	9.6	6.6	15.7	10.7	3.81	3.1
Pyrope	5.11	8.8	7.1	15.9	20.8	11.3	13.9	20.06	18.1
Spessartine	7.08	9.2	8.5	22.5	2.7	4.4	3.7	1.06	0.0
Uvarovite	0.02	0.0	0.0	0.0	0.0	0.0	0.0	0.04	0.0
% cations	98.71	96.9	96.5	97.2	96.6	98.1	95.8	99.50	94.9

**NOTES:** Garnet formula unit and end-member (using Andy Tindle calculator)  
Based on 12 oxygens and with Fe<sup>2+</sup>/Fe<sup>3+</sup> calculated assuming full site occupancy

Table 4. continued

Sample	206352	206354a	206354d	116738	206358	206360a	206360c	206362	206362
Drillhole	WPD04	WPD04	WPD04	WPD04	WPD04	WPD04	WPD04	WPD04	WPD04
Depth	55.0	66.2	66.2	100.0	102.8	108.0	108.0	119.2	119.2
Distance from mineralization (m)	43.4	28.5	28.5	0.0	-1.0	-6.2	-6.2	-17.4	-17.4
Lithology	Amphibolite	Amphibolite	Compositionally layered rock	Disseminated mineralization	Gneiss	Amphibolite	Gneiss	Gneiss	Gneiss
Method	Probe	SEM	SEM	SEM	SEM	SEM	SEM	Probe	SEM
SiO <sub>2</sub>	37.05	39.0	38.7	38.5	39.4	37.1	40.5	37.88	38.9
TiO <sub>2</sub>	0.04	0.0	0.0	0.0	0.0	0.0	0.0	0.02	0.0
Al <sub>2</sub> O <sub>3</sub>	19.96	20.1	19.6	21.3	20.4	20.3	21.0	20.91	19.4
FeO	32.64	24.5	25.3	21.8	30.6	30.4	29.8	33.93	35.1
MnO	3.05	4.0	3.6	9.7	1.2	1.9	1.6	0.47	0.0
MgO	1.25	2.2	1.7	3.9	5.1	2.8	3.4	5.08	4.3
CaO	5.67	10.2	10.8	3.3	3.0	6.6	3.7	2.08	2.3
Na <sub>2</sub> O	0.03	0.0	0.0	0.0	0.4	0.0	0.0	0.03	0.0
K <sub>2</sub> O	0.00	0.0	0.0	0.0	0.2	0.0	0.0	0.01	0.0
ZnO	0.01	0.0	0.1	0.4	0.1	0.0	0.1	0.02	0.0
Cr <sub>2</sub> O <sub>3</sub>	0.01	0.0	0.0	0.0	0.0	0.0	0.0	0.01	0.0
SO <sub>3</sub>	0.00	0.0	0.0	1.1	0.0	0.9	0.0	0.00	0.0
TOTAL	99.71	100.0	100.0	100.0	100.4	100.0	100.0	100.4	100.0
Almandine	71.13	52.1	52.5	52.0	67.8	64.9	71.7	72.97	74.9
Andradite	3.11	3.7	4.7	0.0	2.1	3.7	0.0	2.06	4.0
Grossular	13.54	26.1	27.2	9.6	6.6	15.7	10.7	3.81	3.1
Pyrope	5.11	8.8	7.1	15.9	20.8	11.3	13.9	20.06	18.1
Spessartine	7.08	9.2	8.5	22.5	2.7	4.4	3.7	1.06	0.0
Uvarovite	0.02	0.0	0.0	0.0	0.0	0.0	0.0	0.04	0.0
% cations	98.71	96.9	96.5	97.2	96.6	98.1	95.8	99.50	94.9

**NOTES:** Garnet formula unit and end-member (using Andy Tindle calculator)  
Based on 12 oxygens and with Fe<sup>2+</sup>/Fe<sup>3+</sup> calculated assuming full site occupancy

**Table 5. Electron microprobe and SEM analyses of staurolite from Wheatley**

Sample	206362	206362	206367	206805A
Drillhole	WPD04	WPD04	WPD04	WPD02
Depth	119.9	119.9	174.7	180.8
Distance from main mineralization	-17.4	-17.4	-72.9	-1.8
Method	Probe	SEM	SEM	SEM
SiO <sub>2</sub>	27.30	29.8	35.1	28.9
TiO <sub>2</sub>	0.49	0.0	0.0	0.0
ZnO	0.48	0.4	0.1	0.2
Al <sub>2</sub> O <sub>3</sub>	52.68	52.9	49.1	53.3
Cr <sub>2</sub> O <sub>3</sub>	0.02	0.0	0.0	0.0
FeO	13.90	14.4	13.4	14.6
MnO	0.05	0.0	0.0	0.1
MgO	2.10	2.6	2.2	2.8
CaO	0.00	0.0	0.0	0.0
Na <sub>2</sub> O	0.02	0.0	0.0	0.0
K <sub>2</sub> O	0.00	0.0	0.0	0.0
TOTAL	97.04	100.0	100.0	100.0

**Figure 30. Downhole match for staurolite in WPD04 with SWIR spectra of staurolite from the United States Geological Survey (USGS) spectral library and with the TIR spectra from the John Hopkins University (JHU) spectral library vs simplified log**

## Sillimanite

Similarly for kyanite, the HyLogger cannot be used to show the distribution of sillimanite in the drillhole. Petrological examination showed that fibrous sillimanite (fibrolite) is generally restricted to gneiss close to mineralization (within 5 m) at the Kingsley Prospect (Fig. 10e), although rare coarser grained crystals of sillimanite (Fig. 10d) are present up to 20 m below mineralization. Sillimanite was identified on the basis of its crystal form, high relief, moderate to high birefringence (up to second order blue) and straight extinction. Duplicate microprobe analyses of one of the larger crystals is given in Table 6.

**Table 6. Electron microprobe analyses of sillimanite from Wheatley**

Sample	206362	206362
SiO <sub>2</sub>	36.55	36.55
TiO <sub>2</sub>	0.00	0.00
Al <sub>2</sub> O <sub>3</sub>	62.71	62.62
Cr <sub>2</sub> O <sub>3</sub>	0.03	0.01
FeO	0.52	0.49
MnO	0.02	0.00
MgO	0.01	0.01
CaO	0.00	0.00
Na <sub>2</sub> O	0.02	0.01
K <sub>2</sub> O	0.00	0.01
TOTAL	99.86	99.69

## Andalusite

Andalusite was only observed in a sample from 43 m below mineralization in WPD02 in a layered rock that also consisted of microcline, plagioclase, biotite, quartz and minor tourmaline (Fig. 20). Andalusite was identified on the basis of its high relief, low birefringence (first order yellow), parallel extinction and length-fast character.

## Amphiboles

The calcium-rich amphibole hornblende is abundant in the Wheatley core. Hornblende constitutes a significant component of the amphibolites, compositionally layered rocks and mafic gneisses as well as later mafic intrusions. Hornblende is also present in gneiss beneath the mineralization in WPD07. Hornblende is readily identified by its optical properties but a couple of analyses were made using SEM. The data are included in Table 7. The calcium-poor amphibole cummingtonite was observed intergrown with sulfides in the lower mineralized horizon in WPD04 (Fig. 5c) and its identity confirmed by a combination of its optical properties and SEM and electron microprobe analysis (Table 7). Gedrite has overgrown hornblende beneath the mineralized zone in WPD07 (Fig. 15b) and its identity was confirmed by SEM (Table 7).

**Table 7. Electron microprobe and SEM analyses of amphiboles from Wheatley**

Sample	116738	116738	206369	206369	206369	206370	206370	116766	116766	116766	116766
Drillhole	WPD04	WPD04	WPD04	WPD04	WPD04	WPD04	WPD04	WPD07	WPD07	WPD07	WPD07
Depth (m)	100.00	100.00	178.80	178.80	178.80	180.60	180.60	123.00	123.00	123.00	123.00
Method	SEM	SEM	SEM	SEM	SEM	Probe	Probe	SEM	SEM	SEM	SEM
Mineral	Hornblende	Hornblende	Cummingtonite	Cummingtonite	Cummingtonite	Cummingtonite	Cummingtonite	Gedrite	Gedrite	Gedrite	Gedrite
SiO <sub>2</sub>	43.1	42.5	53.4	54.8	54.6	53.88	53.77	43.9	46.7	47.4	45.8
TiO <sub>2</sub>	0.0	0.0	0.0	0.0	0.0	0.01	0.02	0.0	0.0	0.0	0.0
Al <sub>2</sub> O <sub>3</sub>	15.5	15.5	1.9	1.5	2.1	1.02	0.94	16.6	14.9	14.2	14.7
FeO	16.4	16.8	23.7	22.6	22.3	23.68	23.97	15.6	20.0	20.1	21.3
MnO	0.3	0.4	0.7	0.7	0.6	0.16	0.12	0.0	0.0	0.0	0.0
MgO	9.3	9.4	17.9	18.3	18.1	17.93	17.87	10.9	15.4	15.3	15.1
CaO	12.2	12.5	0.8	0.6	1.3	0.32	0.36	10.7	0.8	0.7	0.8
Na <sub>2</sub> O	2.0	1.8	0.0	0.0	0.0	0.04	0.04	2.3	2.1	2.1	2.2
K <sub>2</sub> O	0.6	1.8	0.0	0.0	0.0	0.00	0.01	0.0	0.0	0.0	0.0
TOTAL	99.4	100.7	98.4	98.6	99.0	97.0	97.1	99.9	99.8	99.9	99.9

## Discussion

### Protoliths of the host succession

#### Amphibolite

Trace element geochemistry confirms that the amphibolite in the hangingwall and footwall at the Kingsley Prospect is basaltic to basaltic andesite in composition (Fig. 26).

#### Compositionally layered rocks

The compositionally layered rocks appear to have preserved original bedding (Fig. 7a) and were interpreted by Griggs (2004) as metamorphosed quartz arenite and arkose. However, the abundance of hornblende in the dark-coloured layers and plagioclase in the light-coloured layers (Fig. 7b) does not support this interpretation. It is far more likely that these rocks represent metamorphosed waterlain mafic tuffs deposited subaqueously with the layering due to difference in settling rates or mechanical sorting of the minerals. The lighter quartz-rich layers possibly indicate some clastic input.

#### ?Felsic volcanic and volcanic breccia

The fine-grained light-grey rock composed of quartz, microcline, plagioclase, biotite, white mica and minor tourmaline at the bottom of the WPD07 and WPD02 drillholes (Fig. 16a) and associated fragmental rock (Fig. 16b,c,d) were interpreted by Johnston (2003) and Griggs (2004) to be felsic volcanic or pyroclastic rock. Similar rocks interlayered with quartzite, banded iron-formation (BIF) and quartz–feldspar–biotite gneiss between Balingup and Bridgetown were described as granofels by Wilde (1980) and were interpreted to have been derived from metamorphosed psammopelitic greywackes. A sample from WPD02 taken for dating by Sircombe et al. (2007) was interpreted to be a metapsammite with a minimum age of deposition of about 2646 Ma. Given the abundance of microcline, plagioclase and micas in the sample analysed by Sircombe et al. (2007), it is considered more likely that this rock is a metamorphosed felsic volcanic rock, and the c. 2646 Ma age is then the age of eruption.

#### Felsic gneiss

Determining the protolith of the quartz–biotite–garnet  $\pm$  plagioclase  $\pm$  staurolite  $\pm$  sillimanite  $\pm$  kyanite gneiss that underlies the Kingsley Prospect mineralization is critical for determining the tectonic environment under which the mineralization formed. Unfortunately, alteration and metamorphism has destroyed all primary textures within the gneiss making this task very difficult.

Quartz–feldspar–biotite  $\pm$  garnet gneiss interlayered with thin units of quartzite and BIF is extensively developed in the Balingup complex and was interpreted by Wilde (1980) as probably derived from arkosic sediments.

However, gneiss of this composition could equally have been formed by metamorphism of felsic volcanic or volcanoclastic rocks, particularly if these rocks had been altered prior to metamorphism.

#### Tectonic setting

Any model for tectonic setting at Wheatley needs to take into account the widespread quartz–feldspar–biotite gneiss within the Balingup complex and the local presence of compositionally layered hornblende-rich rocks and amphibolites at Wheatley. If the gneisses underlying the mineralization at Wheatley were sedimentary in origin, as interpreted by Wilde (1980), then the large amount of feldspar within them would imply very rapid erosion and deposition or deposition close to source. Rapid sedimentation from a continental source into a graben would not explain the presence of compositionally layered hornblende-bearing rocks above the mineralization at Wheatley and in places interlayered with the gneisses below mineralization, nor would it explain the presence of amphibolites. A model involving active volcanism would better explain the rock types observed with layering resulting from mechanical separation of phases during subaqueous deposition.

The amphibolites have the least ambiguous protolith of all the rock types with a basaltic to basaltic andesite composition. Their protoliths could either have been basalt flows or intrusions. However, most amphibolite forms layers parallel with what is interpreted here as sedimentary layering, and on this basis an extrusive origin for the protolith is preferred. They are foliated and thus pre-dated deformation. Where metamorphism is below amphibolite grade, a Th/Yb vs Nb/Yb plot is useful for discriminating basalts contaminated by continental crust (steep trends) from those related to melting of a subduction-modified mantle source (trends parallel with a mantle-ocean island basalt (OIB) array; Fig. 31; Pearce, 2008). However, mobility of Th during high-grade metamorphism can result in an almost vertical data trend (Pearce, 2008). This may be the reason for the apparent vertical trend shown by the amphibolites at the Kingsley Prospect (Fig. 31). Similarly, metamorphic enrichment in Th could have resulted in most of the amphibolites plotting in the volcanic arc basalt to calc-alkaline basalt field of Wood (1980), whereas the three samples located within or close to the MORB–OIB array in terms of the Th/Yb vs Nb/Yb plot fall in the E-MORB–WPB (within plate basalt) fields of Wood (1980; Fig. 32). The three samples that fall within or close to the MORB–OIB array on the Th/Yb vs Nb/Yb plot have very flat patterns on the mantle-normalized immobile element plot (Fig. 28a) suggesting an enriched MORB (close to E-MORB) protolith. The amphibolite from the Jack Prospect has a much lower Nb/Yb ratio and could have resulted from crustal contamination of N-MORB magma.

Black smokers on mid-ocean ridges are currently forming massive sulfide deposits although these deposits are poorly represented in the geologic record because ridges typically are subducted (Hannington et al., 2005). However, basalts with MORB-type signatures are present in many types of



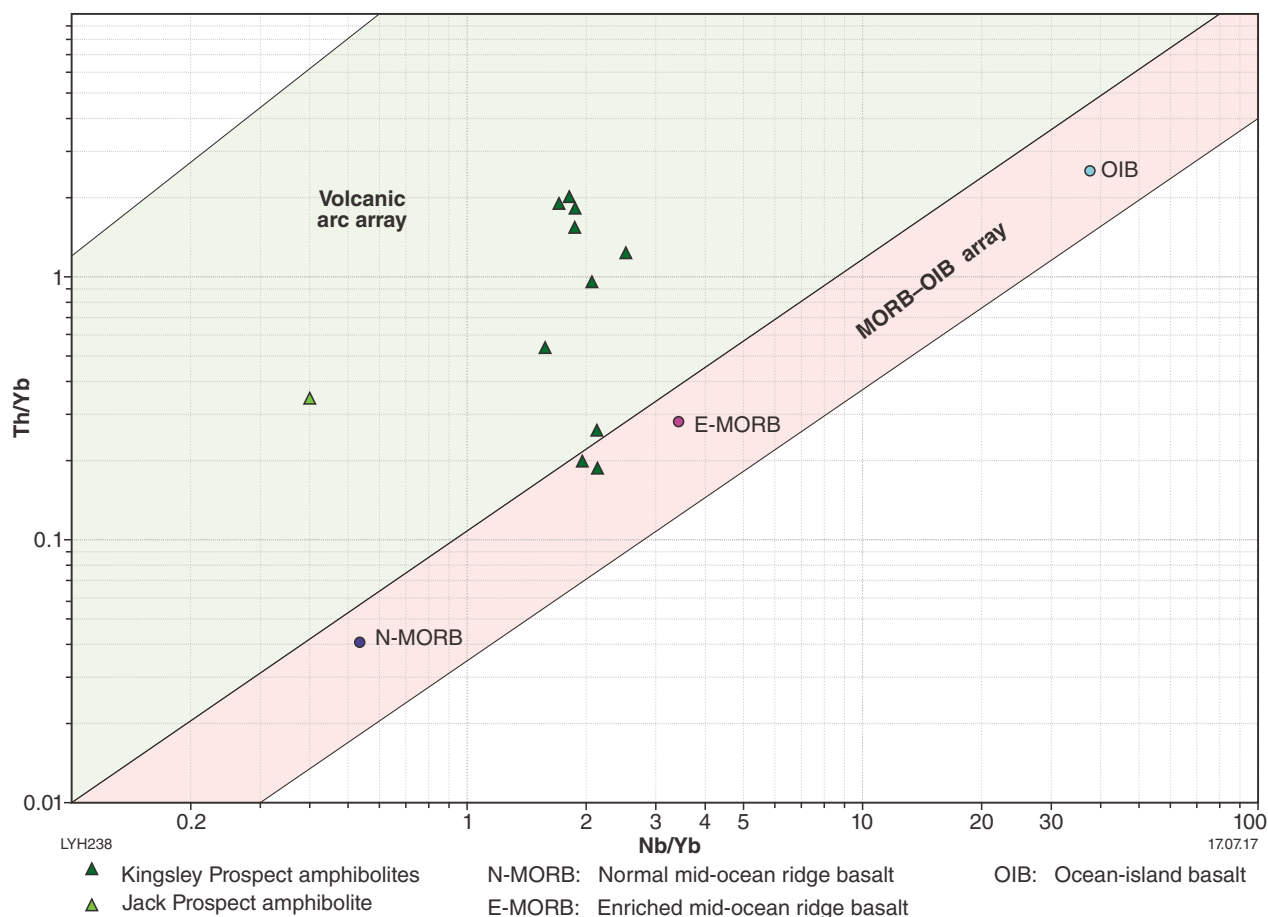


Figure 31. Amphiolites plotted on Th/Yb vs Nb/Yb discrimination plot of Pearce (2008)

VMS deposit where there is high-temperature magmatic activity in an extensional geodynamic environment including back-arc basins and intra-arc rifts (Piercey, 2007, 2011). Bimodal felsic and siliciclastic–felsic VMS deposits in evolved continental arc to back-arc environments commonly have MORB-like basalt overlying or crosscutting felsic volcanic and intrusive rocks. The MORB-like basalts in evolved environments are commonly E-MORB in composition and form through mantle-decompression melting as asthenosphere upwells beneath zones of arc-rifting and back-arc spreading (Piercey, 2011). Mineralization is far more likely to be preserved within a back-arc basin than in a mid-ocean ridge spreading centre (Hannington et al., 2005).

A rifted back-arc basin setting would account for the abundance of felsic gneiss and also the presence of the compositionally layered rocks above mineralization as explosive volcanism in the arc could have provided the source of the material.

## Morphology of the mineralization

The remarkable continuity of the main horizon of base-metal mineralization at the Kingsley Prospect over a

strike length of at least 1.6 km, at or close to the boundary between felsic gneiss and a series of amphiolites and compositionally layered rocks, indicates a strong stratigraphic control for the mineralization. While it is possible that the mineralization is hydrothermal and formed along a permeable boundary between the two units subsequent to deposition or a shear zone separating the two rock types, this is considered unlikely as wallrock alteration under these conditions would be expected to be symmetrical whereas the alteration at Wheatley is below the mineralized zone (see following section). Furthermore, if the mineralization was along a major fault zone, significant quartz or carbonate veining would be expected but quartz veining at Wheatley is minor and post-dates foliation. It is more likely that the mineralization is syngenetic. The association with metavolcanic rocks is consistent with a VMS origin for the mineralization rather than a sedimentary exhalative (SEDEX) origin. Lydon (1984) noted that clusters of VMS deposits in the Noranda, Matagami and Bathurst areas of Canada and the Green Tuff Belt of Japan tended to occur within a single stratigraphic interval, referred to as the 'favourable horizon'. However, some VMS-bearing districts, such as Golden Grove in the Murchison region of Western Australia, have mineralization at more than one horizon

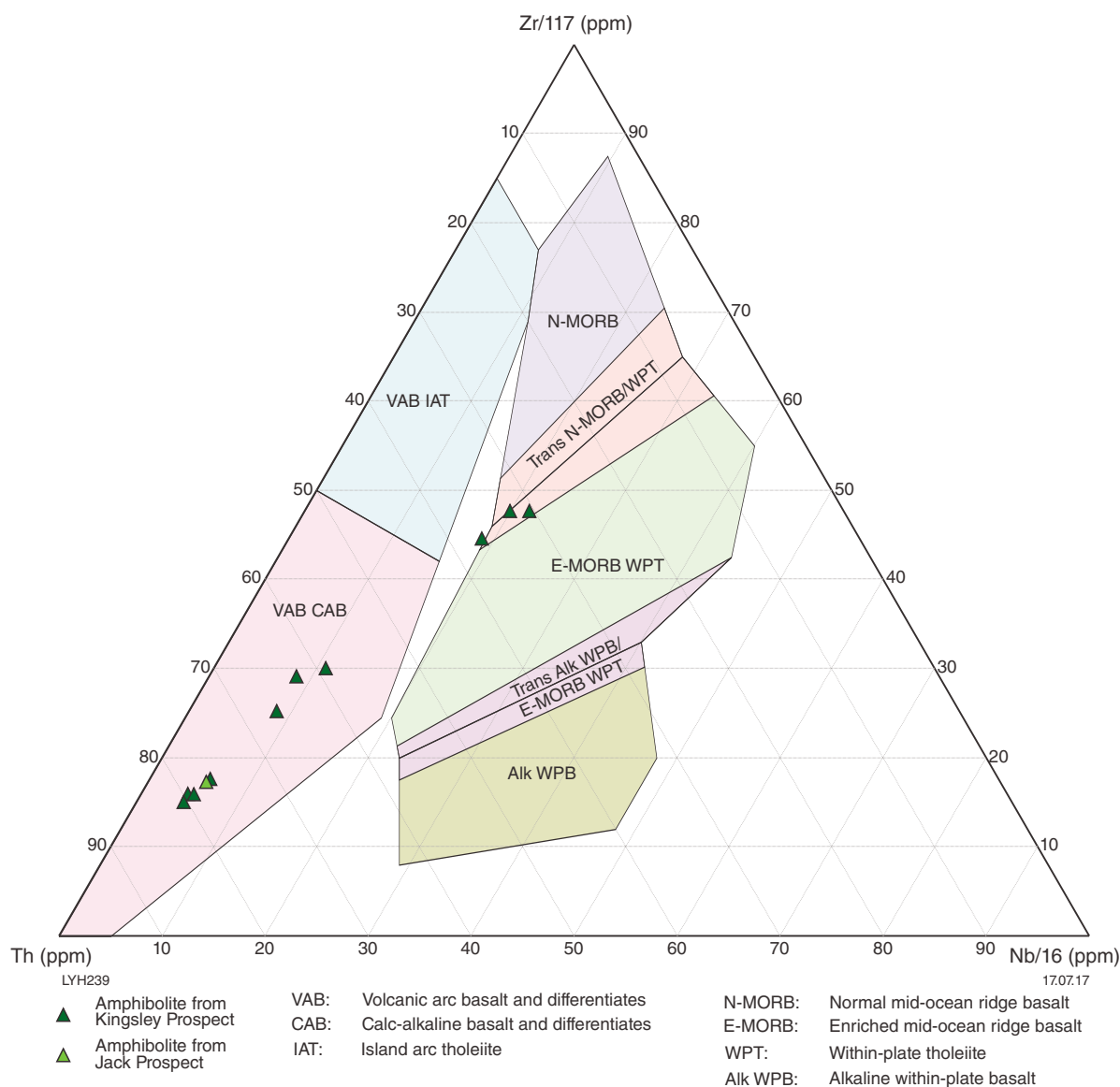


Figure 32. Amphibolites plotted on Th–Zr–Nb discrimination plot of Wood (1980)

(Clifford, 1992). A second mineralized horizon was recognized in WPD04 but not in the other drillholes from the Kingsley Prospect.

Mineralization intersected in WPD03 from the Jack Prospect consisted of fracture filling in a layered mafic intrusion. It is possible that it represents remobilized VMS mineralization. However, it is more likely that it represents mobilization of primary magmatic sulfides in the intrusion, given the association of pentlandite with the pyrrhotite.

## Evidence of alteration

Footwall alteration is a characteristic feature of VMS deposits. In unmetamorphosed to upper greenschist facies examples, alteration generally occurs either as a pipe that typically has an inner zone of chlorite and an outer zone of

sericite or as a broad, diffuse, semiconformable chloritic and sericitic alteration zone (Sangster, 1972; Gibson and Kerr, 1993; Gibson and Galley, 2007). Carbonate and argillic alteration may also be present (Gibson et al., 1999). Talc has also been reported as a footwall alteration mineral at Mattagami Lake (Roberts and Rearden, 1978; Costa et al., 1983) and Noranda (Gibson and Galley, 2007) in Canada and at the Yuinmery VMS prospects including Just Desserts in the northwestern Youanmi Terrane of Western Australia (Hassan, 2014). During metamorphism, chlorite (especially chlorite with moderate to high Fe/Fe+Mg ratio) becomes unstable and the original chloritic alteration assemblage may be altered to become an assemblage consisting of hornblende, biotite, cordierite and anthophyllite. If sufficient calcite were present, tremolite–actinolite, garnet and Ca-pyroxenes may also form (Sangster, 1972).

Kyanite, andalusite, sillimanite and staurolite may form as a result of metamorphism of alteration associated with VMS mineralization. For example, kyanite has been recognized in ore and veins at the following deposits:

- Mattabi deposit in Canada (Franklin, 1975)
- associated with metamorphosed Al–Si alteration in VMS deposits at the Savant Lake, Marshall Lake and Manitouwadge VMS deposits in Ontario, Canada (Pan and Fleet, 1999)
- Snow Lake, Manitoba (Zaleski et al., 1991; Caté et al., 2015)
- Teutonic Bore in the Eastern Goldfields of Western Australia (Greig, 1984)
- in the distal alteration zone of VMS deposits at Quinns, in the Murchison region of Western Australia (Duuring et al., 2016).

Andalusite is associated with the following:

- Al–Si alteration at Savant Lake, Ontario (Pan and Fleet, 1999)
- in the silicified zone beneath ore at Mattabi as well as in the hangingwall and footwall (Franklin, 1975)
- in altered mafic volcanics beneath mineralization at Teutonic Bore (Greig, 1984)
- in the distal alteration zone at Quinns (Duuring et al., 2016).

Sillimanite is also associated with Al–Si alteration beneath VMS mineralization at Savant Lake, Marshall Lake and Manitouwadge, Ontario (Pan and Fleet, 1999) and Snow Lake, Manitoba (Caté et al., 2015). It is unusual for all three polymorphs of aluminium silicate to be present in the same deposit; however, they have been reported from Savant Lake and Marshall Lake in Canada (Pan and Fleet, 1999). At Wheatley, andalusite was only identified in one section distal from mineralization and was not associated with kyanite or sillimanite.

Staurolite is related to Fe–Zn–Mg–Al alteration proximal to mineralization at Snow Lake, Manitoba (Zaleski et al., 1991; Caté et al., 2015) and is present up to 30 m above and below mineralization at Hollandaire, in the Murchison region of Western Australia (Hayman et al., 2015).

At the Kingsley Prospect, the quartz–biotite–garnet  $\pm$  kyanite  $\pm$  sillimanite  $\pm$  staurolite gneiss located beneath mineralization was interpreted by Johnston (2003) and Griggs (2004) as metamorphosed footwall alteration. Griggs (2004) interpreted the rocks above and below mineralization to be metamorphosed quartz arenite and arkose with the garnet, biotite, sillimanite and staurolite below mineralization being the result of alteration. However, he did consider the possibility that the aluminosilicates could alternatively reflect a pelitic primary protolith. Given that the compositionally layered rocks above mineralization contain an abundance of hornblende, it is unlikely that they had a quartz arenite or

arkosic protolith, as discussed above, and are more likely to be metamorphosed mafic tuffs. Where mineralization is hosted within mafic rocks rather than in felsic gneiss as in WPD07, gedrite and phlogopite replace hornblende in the footwall. The gneisses immediately below the gedrite-bearing zone contain garnet, staurolite and sillimanite.

Wilde (1980) noted that aluminosilicates are largely absent from the metamorphosed rocks regionally except for the rare occurrence of kyanite and staurolite near Bridgetown. This would imply that the gneisses containing aluminosilicates around the Wheatley area either had a more pelitic protolith or that they had undergone alteration. However, it is more probable that the kyanite, sillimanite and staurolite are the result of metamorphism of an argillic alteration zone within felsic volcanic or volcanoclastic rocks. The presence of hornblende-rich compositionally layered rock interlayered with felsic gneiss below mineralization in WPD02 (and possibly also in WPD07, if it is not unfaulted) is evidence that these rock types have different protoliths. The composition of the garnet in the compositionally layered rocks above and below mineralization (almandine with significant grossular and some spessartine) is similar to that in the amphibolites but is quite distinct from that in the felsic gneiss (almandine with some pyrope) as previously described, providing further evidence that these intervals represent different protoliths.

The composition of garnet does not provide clear evidence of Mn metasomatism as it is largely controlled by the composition of the protolith. However, the high content of spessartine in one garnet sample from disseminated mineralization does suggest that Mn was introduced with mineralization.

The presence of abundant tourmaline in the footwall beneath sulfide mineralization in WPD02 (Fig. 19a,b) as well as the presence of disseminated tourmaline in other footwall rocks (Figs 16d, 20) indicates that boron was introduced. Tourmaline is associated with many VMS deposits and is interpreted to have originated through submarine hydrothermal exhalative activity or sea floor replacement processes with regional metamorphism contributing to recrystallization of tourmaline (Slack, 2012). It is likely that boron alteration was related to volcanic exhalative activity at the time of mineralization at the Kingsley Prospect. A later replacement origin related to the tourmaline-bearing pegmatites that intrude the succession cannot be ruled out but there is no evidence of a spatial relationship between the occurrence of tourmaline and the pegmatites.

## Evidence for pre-metamorphic origin of the mineralization

Gahnite is present in many metamorphosed VMS deposits and is interpreted to have formed by reaction between sphalerite and aluminous silicates (Sangster, 1972). Its presence at the Kingsley Prospect is a clear indication that the sulfides pre-dated metamorphism and this supports a VMS origin for the sulfides.

## Age of mineralization

Two weakly mineralized samples from Wheatley gave model Pb/Pb ages of c. 2690 and 2710 Ma respectively (Denton et al., 2003) whereas U–Pb SHRIMP dating gave a maximum age of formation of rock (interpreted to be a metasediment by Denton et al. [2003] but here interpreted to be a felsic volcanic rock) below mineralization of c. 2646 Ma. Given the errors involved in calculating model Pb/Pb ages, an age of mineralization of c. 2646 Ma is probable. Hollis et al. (2015) noted that there are four major periods of VMS formation in the Youanmi Terrane: >2900 Ma (e.g. Golden Grove), c. 2815 Ma (e.g. Austin), 2760–2745 Ma (e.g. Hollandaire) and c. 2725 (e.g. Gum Creek greenstone belt), and in the Eastern Goldfields VMS mineralization formed between c. 2700 and 2680 Ma (e.g. Teutonic Bore). The Wheatley mineralization is thus younger than all other VMS mineralization in the Yilgarn and indicates another period when VMS mineralization took place.

## Uses and limitations of the HyLogger data

The HyLogger is good at identifying major mineralogical changes down the scanned drillholes. For example, the intervals interpreted to be felsic volcanic rocks at the bottom of WPD07 and WPD02 are clearly identified by the presence of abundant micas in the SWIR summary plot (Figs 14b, 18b), and the post-peak metamorphic gabbro in WPD02 is clearly identified by low quartz content and abundant plagioclase, pyroxene and amphibole in the TIR summary plot (Fig. 18a).

TIR spectra also showed a change in the composition of the garnet down the drillholes. Even though electron microprobe and SEM analysis indicated that the HyLogger had overestimated the amount of grossular and spessartine in the garnet and that almost all garnet was almandine, a trend to more grossular, and spessartine-rich garnet in the mafic rocks was detected (see section on mineral distribution and chemistry).

Matching of detected spectra with spectra from external libraries can be useful but care is needed. For example, in the matching of spectra with the SWIR spectra of staurolite from the USGS spectral library and with the TIR spectra of staurolite from JHU spectral library for WPD04, both showed staurolite as being concentrated in the felsic gneiss. However, the SWIR match shows staurolite as being much more abundant (Fig. 30) and may have been influenced by other minerals such as biotite. A match of kyanite with the SWIR spectra of staurolite from the USGS spectral library simply identified white mica as the kyanite in the spectral library that must have been altering to white mica.

The zone of massive tourmaline in WPD02 (Fig. 19a,b) does not show up in weighted plots of tourmaline for SWIR or TIR spectra (Fig. 33). Even though there is a good visual match of the SWIR spectra with Fe-tourmaline (Fig. 34), the automatically generated interpretation from the TSG software is that it is aspectral.

Tourmaline is detected in the pegmatites and possible felsic volcanic rocks at the bottom of the WPD02 drillhole in the SWIR plot. This is possibly because the zone of massive tourmaline is very dark whereas the other tourmaline-bearing rocks are light coloured. However, the TIR weighted plot of tourmaline shows tourmaline in places where it was not observed but not in places where it was (Fig. 33) and the plot is thus considered unreliable.

## Exploration vectors

Although zinc-bearing spinel can occur in a range of rock types including aluminous sediments, marble and pegmatites, gahnite is more diagnostic of strongly zinc-rich lithologies such as VMS and sedimentary exhalative (SEDEX) deposits (Spry and Scott, 1986). Gahnite at the Kingsley Prospect is intimately associated with the mineralization and is clearly genetically related to it. Thus, the presence of gahnite in stream samples is a good indicator of the presence of VMS mineralization. Gahnite from a stream sediment sample obtained by BHP Minerals Ltd (Hart et al., 2000) from a creek 2.4 km north of the Kingsley Prospect is compositionally similar to that from the Kingsley Prospect. As branches of this creek drain the possible northern and southern extensions of the Kingsley Prospect, it is possible that the gahnite was derived from that source. However, the sample site is located only 770 m southwest of the Jack Prospect (WPD03) and 800 m west of historic eluvial kyanite workings. WPD03 failed to intersect VMS mineralization and the only mineralization present is in fractures within a layered mafic intrusion. However, it is possible that VMS mineralization in the vicinity of WPD03 was removed during emplacement of the layered mafic intrusive, and that elsewhere in the area VMS mineralization is still present.

The occurrence of massive coarse-grained eluvial kyanite in the vicinity is also potentially a vector to metamorphosed argillic alteration related to VMS mineralization. Kyanite is significantly more abundant around the old workings than at the Kingsley Prospect which could suggest the potential for higher grade mineralization than that intersected at the Kingsley Prospect.

Staurolite in stream samples is another potential vector to VMS mineralization. Zinc-rich staurolite is associated with gahnite at the Linda VMS deposit, Snow Lake, Manitoba, Canada (Zaleski, 1991). The staurolite from Kingsley is not as zinc rich as that from the Linda deposit but does contain up to 0.4% Zn.

Garnet chemistry was tested as a vector towards mineralization; however, it is demonstrated that its chemistry is more closely related to composition of the protolith at the Kingsley Prospect rather than solely reflecting rock-alteration patterns. However, garnets with more than 20% spessartine are likely to be related to mineralization as the only garnet with more than 20% spessartine was in mineralized gneiss.

Laterite lag sampling has already been used with limited success in the Wheatley area. Apart from the base metals, Bi may be a useful indicator of mineralization as native bismuth was commonly observed as inclusions in galena.



Figure 33. Weighted downhole distribution of tourmaline in WPD02: a) simplified log; b) SWIR spectra; c) TIR spectra

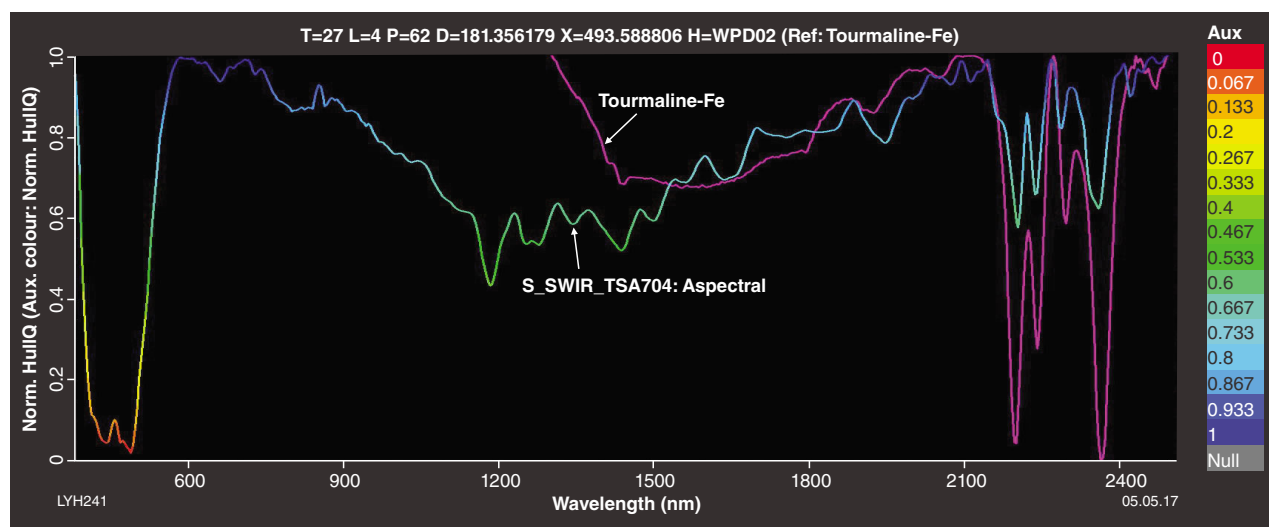


Figure 34. Spectra over zone of massive tourmaline in WPD02 compared with the SWIR spectra for Fe-tourmaline in TSG

Drilling of EM anomalies successfully located mineralization at the Kingsley Prospect. Some EM anomalies outlined by BHP Minerals (Hart et al., 2000) have yet to be adequately tested.

## Conclusions

A VMS origin for the mineralization at the Kingsley Prospect is supported by the presence of gahnite which indicates that mineralization pre-dates amphibolite facies metamorphism, and by the strong stratigraphic control of mineralization at or close to the contact between gneisses of felsic composition and an overlying more mafic assemblage of compositionally layered rocks and amphibolites. The presence of sillimanite, kyanite, staurolite and garnet in the underlying gneisses are all consistent with metamorphosed argillic alteration, and the presence of tourmaline is also indicative of boron metasomatism. Garnet composition is generally related to host-rock composition with garnet in felsic gneiss being predominantly almandine with minor pyrope and mafic rocks containing a higher proportion of grossular and some spessartine. However, the highest spessartine was recorded in mineralized rocks suggesting some Mn metasomatism.

The mineralization intersected at the Jack Prospect is interpreted to have formed post-peak metamorphism within fractures in a layered mafic intrusion. However, the presence of gahnite in a creek sample close to the Jack Prospect as well as the presence of coarse-grained eluvial kyanite could indicate potential for more VMS mineralization in the area. Bismuth in laterite may also be a useful pathfinder to mineralization.

The layered mafic intrusion at the Jack Prospect and mafic intrusions at the Kingsley Prospect may be indicative of a magma chamber that provided a source of long-lived high heat flow in the area which would be essential for driving a high-temperature hydrothermal system.

The E-MORB-like trace element chemistry of some of the amphibolites overlying the Kingsley mineralization indicates that they were formed at high temperature in an extensional environment. This is consistent with mineralization taking place in a rifted back-arc basin. The high Th/Yb ratio in the other amphibolites could be due to variable crustal contamination (perhaps related to subduction) or gain of Th during metamorphism.

Considerably more work, including seismic surveys, trace element geochemistry and geochronology across the region is required to verify the tectonic setting and further constrain indicators for VMS deposits. Local exploration vectors include the presence of gahnite and Zn-bearing staurolite in stream sediments, laterite geochemistry (in particular, laterite with high concentrations of Bi) and EM anomalies.

## Acknowledgements

Hampton Hill Mining Ltd is thanked for donating diamond drillcore to GSWA, and for providing unpublished lead isotope data from the Wheatley project. Malcom Roberts from the Centre for Microscopy, Characterisation and Analysis, The University of Western Australia is thanked for assisting with electron microprobe analyses and Michael Verrall from the Earth Science and Resource Engineering division of CSIRO at Kensington is thanked for assisting with SEM analyses. Jon Huntington, Scott Halley, and Lena Hancock are thanked for demonstrating techniques that show variation in mineral chemistry using HyLogger data. Hugh Smithies, Paul Duuring and Simon Johnson are thanked for reviewing this report and suggesting many improvements.

## References

- Carlson, RD and Harrison, PH 1993, South West project, annual report to 16th December 1993, E70/167 (Yanmah), E70/631 (Mt Mack), E70/946 (Wilgarup), E70/869 (Smithfield) (SI 50-10); Pancontinental Mining Limited: Geological Survey of Western Australia, Statutory mineral exploration report, A40133, 61p.
- Cassidy, KF, Champion, DC, Krapež, B, Barley, ME, Brown, SJA, Blewett, RS, Groenewald, PB and Tyler, IM 2006, A revised geological framework for the Yilgarn Craton, Western Australia: Geological Survey of Western Australia, Record 2006/8, 8p.
- Caté, A, Mercier-Langevin, P, Ross, P-S, Duff, S, Hannington, MD, Dubé, B and Gagné, S 2015, Geology and Au enrichment processes at the Paleoproterozoic Lalor auriferous volcanogenic massive sulphide deposit, Snow Lake Manitoba, *in* Targeted geoscience initiative 4: contributions to the understanding of volcanogenic massive sulphide deposit genesis and exploration methods development *edited by* JM Peter and P Mercier-Langevin: Geological Survey of Canada, Canada Open File 7853, p. 131–145.
- Clifford, BA 1992, Facies and palaeoenvironment analysis of the Archaean volcanic-sedimentary succession hosting the Golden Grove Cu–Zn massive sulphide deposits, Western Australia: Monash University, PhD thesis (unpublished), 343p.
- Costa, UR, Barnett, RL and Kerrich, R 1983, The Mattami Lake Mine Archean Zn–Cu sulfide deposit, Quebec: hydrothermal coprecipitation of talc and sulfides in a sea-floor brine pool - evidence from geochemistry,  $^{18}\text{O}/^{16}\text{O}$ , and mineral chemistry: *Economic Geology*, v. 78, p. 1144–1203.
- Denton, GJ, Carr, GR, Korsh, MJ and Gardner, BL 2003, Metallogenic aspects of two drill sample pulps from the Wheatley prospect, southern Yilgarn Block, Western Australia, based on their Pb isotopic composition: Unpublished report for Teck Cominco Australia Pty Ltd, 2p.
- Donovan, JJ and Tingle, TN 1996, An improved mean atomic number correction for quantitative microanalysis: *Journal of Microscopy*, v. 2, p. 1–7.
- Duuring, P, Hassan, L, Zelic, M and Gessner, K 2016, Geochemical and spectral footprint of metamorphosed and deformed VMS-style mineralization in the Quinns District, Yilgarn Craton, Western Australia: *Economic Geology*, v. 111, no. 6, p. 1411–1438.
- Ellis, HA 1948, The Yanmah kyanite deposit, Mineral Claim 287H, *in* Report of the Geological Survey for the year 1947: Geological Survey of Western Australia, Perth, Western Australia, p. 6–7.

- Fletcher, IR, Wilde, SA, Libby, WG and Rosman, KJR 1983, Sm–Nd model ages across the margins of the Archaean Yilgarn Block, Western Australia — II; southwest transect into the Proterozoic Albany–Fraser Province: *Journal of the Geological Society of Australia*, v. 30, p. 333–340.
- Gee, RD, Baxter, JL, Wilde, SA and Williams, IR 1981, Crustal Development in the Archaean Yilgarn Block, Western Australia: Geological Society of Australia, Special Publication 7, p. 43–56.
- Gibson, HL and Galley, AG 2007, Volcanogenic massive sulphide deposits of the Archean, Noranda district, Quebec, *in* Mineral deposits of Canada: a synthesis of major deposit-types, district metallogeny, the evolution of geological provinces, and exploration methods *edited by* WD Goodfellow: Geological Association of Canada, Special Publication 5, p. 533–552.
- Gibson, HL and Kerr, DJ 1993, Giant volcanic-associated massive sulfide deposits: with emphasis on Archean examples, *in* Giant ore deposits *edited by* BH Whiting, CJ Hodgson and R Mason: Society of Economic Geologists, Special publication 2, p. 319–348.
- Gibson, HL, Morton, RL and Hudak, GJ 1999, Submarine volcanic processes, deposits, and environments favourable for the location of volcanic-associated massive sulfide deposits, *in* Volcanic-hosted massive sulfide deposits: processes and examples in modern and ancient settings *edited by* CT Barrie and MD Hannington: Society of Economic Geologists, Reviews in Economic Geology 8, p. 13–51.
- Greig, DD 1984, Geology of the Teutonic Bore massive sulfide deposit, Western Australia: Australasian Institute of Mining and Metallurgy Proceedings, v. 289, p. 147–156.
- Griggs, D 2004, Annual Report E70/2258, Wheatley project; Teck Cominco Australia Pty Ltd: Geological Survey of Western Australia, Statutory mineral exploration report, A68682, 14p.
- Günther, D, Quandt, A, Wirz, R, Cousin, H, and Dietrich, VJ 2001, Elemental analyses using laser ablation-inductively coupled plasma-mass spectrometry (LA-ICP-MS) of geological samples fused with  $\text{Li}_2\text{B}_4\text{O}_7$  and calibrated without matrix-matched standards: *Mikrochimica Acta*, 136, p. 101–107.
- Hancock, EA, Green, AA, Huntington, JF, Schodlok, MC and Whitbourn, LB 2013, HyLogger-3: Implications of adding thermal-infrared sensing: Geological Survey of Western Australia, Record 2013/3, 24p.
- Hannington, MD, de Ronde, CEJ and Petersen, S 2005, Sea-floor tectonics and submarine hydrothermal systems, *in* Economic Geology 100th Anniversary Volume *edited by* JW Hedenquist, JFH Thompson, RJ Goldfarb and JP Richards: Society of Economic Geologists, Littleton, Colorado, p. 111–141.
- Hart, J, Smit, R and Stephens, D 2000, First annual report E70/1932, Balingup Gneiss Complex; BHP Minerals Pty Ltd: Geological Survey of Western Australia, Statutory mineral exploration report, A60705, 25p.
- Hassan, LY 1998, Mineral occurrences and exploration potential of southwest Western Australia: Geological Survey of Western Australia, Report 65, 38p.
- Hassan, LY 2014, The Yuinmery volcanogenic massive sulfide prospects: mineralization, metasomatism and geology: Geological Survey of Western Australia, Report 131, 65p.
- Hassan, LY, Ferguson, KM, Cooper, RW, Peiris, EPW and Rogerson, R 1998, Mineralization and geology of southwest Western Australia (1:500 000 scale): Geological Survey of Western Australia, Report 65, Plate 1.
- Hayman, PC, Hull, SE, Cas, RAF, Summerhayes, E, Amelin, Y, Ivanic, TJ and Price, D 2015, A new period of volcanogenic massive sulfide formation in the Yilgarn: a volcanological study of the ca 2.76 Ga Hollandaire VMS deposit, Yilgarn Craton, Western Australia: *Australian Journal of Earth Sciences*, v. 62, p. 189–210.
- Jenner, GA 1996, Trace element geochemistry of igneous rocks: geochemical nomenclature and analytical geochemistry, *in* Trace element geochemistry of volcanic rocks: application for massive sulphide exploration *edited by* DA Wyman: Geological Association of Canada, Short Course Notes 12, p. 51–77.
- Johnston, P 2003, Annual report E70/2258, Wheatley project; Teck Cominco Australia Pty Ltd: Geological Survey of Western Australia, Statutory mineral exploration report, 66807, 13p.
- Kerrick, R and Said, N 2011, Extreme positive Ce-anomalies in a 3.0 Ga submarine volcanic sequence, Murchison Province: Oxygenated marine bottom waters: *Chemical Geology*, v. 280, no. 1, p. 232–241.
- Kerrick, R and Wyman, DA 1997, Review of developments in trace-element fingerprinting of geodynamic settings and their implications for mineral exploration: *Australian Journal of Earth Sciences*, v. 44, no. 4, p. 465–487.
- Lowry, DC, Wilde, SA and Walker, IW 1983, Collie, WA Sheet SI50-6: Geological Survey of Western Australia, 1:250 000 Geological Series.
- Lu, Y, Wingate, MTD and Bodorkos, S 2016, 184116: quartzite, Polina Road; Geochronology Record 1310: Geological Survey of Western Australia, 4p.
- Lu, Y, Wingate, MTD, Bodorkos, S and Wyche, S 2015, 184117: granite gneiss, Brockman Highway; Geochronology Record 1280: Geological Survey of Western Australia, 4p.
- Lydon, JW 1984, Ore deposit models — 8, Volcanogenic massive sulphide deposits, Part 1: a descriptive model: *Geoscience Canada*, v. 11, p. 195–202.
- Morin-Ka, S 2012, Hyperspectral characterization of rare earth minerals: Geological Survey of Western Australia, Record 2012/12, 50p.
- Morris, PA 2007, Composition of the Bunbury Basalt (BB1) and Kerba Monzogranite (KG1) geochemical reference materials, and assessing the contamination effects of mill heads: Geological Survey of Western Australia, Record 2007/14, 22p.
- Myers, JS 1990, Yilgarn Craton — Western Gneiss Terrane, *in* Geology and mineral resources of Western Australia: Geological Survey of Western Australia, Memoir 3, p. 13–32.
- Pan, Y and Fleet, ME 1999, Kyanite in the western Superior Province of Ontario: implications for Archean accretionary tectonics: *The Canadian Mineralogist*, v. 37, p. 359–373.
- Partington, GA, McNaughton, NJ and Williams, IS 1995, A review of the geology, mineralization, and geochronology of the Greenbushes Pegmatite, Western Australia: *Economic Geology*, v. 90, p. 616–635.
- Pearce, JA 1996, A users' guide to basalt discrimination diagrams, *in* Trace element geochemistry of volcanic rocks: applications for massive sulphide exploration *edited by* DA Wyman: Geological Association of Canada, Short Course Notes 12, p. 79–113.
- Pearce, JA 2008, Geochemical fingerprinting of oceanic basalts with applications to ophiolite classification and the search for Archean oceanic crust: *Lithos*, v. 100, p. 14–48.
- Pearce, JA and Cann, JR 1971, Ophiolite origin investigated by discriminant analysis using Ti, Zr and Y: *Earth and Planetary Science Letters*, v. 12, p. 339–349.
- Pearce, JA and Cann, JR 1973, Tectonic setting of basic volcanic rocks determined using trace element geochemistry: *Earth and Planetary Science Letters*, v. 19, p. 290–300.
- Piercey, SJ 2007, An overview of the use of petrochemistry in regional exploration for volcanogenic massive sulfide (VMS) deposits, *in* Proceedings of Exploration 07: Fifth Decennial International Conference on Mineral Exploration *edited by* B Milkereit: Decennial Mineral Exploration Conferences; Exploration 07: exploration in the new millenium, Toronto, Canada, 9 September 2007, p. 223–246.



- Piercey, SJ 2011, The setting, style, and role of magmatism in the formation of volcanogenic massive sulfide deposits: *Mineralium Deposita*, v. 46, p. 449–471.
- Pontual, S 2008, GMEEX spectral analysis guides for mineral exploration (3rd edition): AusSpec International Ltd, 10 vols.
- Roberts, RG and Rearden, EJ 1978, Alteration and ore-forming processes at Mattagami Lake Mine, Quebec: *Canadian Journal of Earth Sciences*, v. 15, p. 1–21.
- Rollinson, HR 1993, Using geochemical data: evaluation, presentation, interpretation: Pearson Education Ltd, Harlow, England, 352p.
- Sangster, DF 1972, Precambrian volcanogenic massive sulphide deposits in Canada: a review: Department of Energy and Resources (Ottawa), 44p.
- Savage, B 2007, Wheatley project, Annual report E70/2258 & E70/2339; Hampton Hill Mining: Geological Survey of Western Australia, Statutory mineral exploration report, A75300, 13p.
- Sircombe, KN, Cassidy, KFC, Champion, DC and Tripp, G 2007, Compilation of SHRIMP U–Pb geochronological data, Yilgarn Craton, Western Australia, 2004–2006: *Geoscience Australia, Geoscience Australia Record 2007/01*, 182p.
- Slack, JF 2012, Exhalites, in *Volcanogenic massive sulfide occurrence model*: US Geological Survey Scientific Investigations Report 2010–5070, no. 10, p. 159–163.
- Spry, PG and Scott, SD 1986, The stability of zincian spinels in sulfide systems and their potential as exploration guides for metamorphosed massive sulfide deposits: *Economic Geology*, v. 81, no. 6, p. 1446–1463.
- Sun, S-S and McDonough, WF 1989, Chemical and isotopic systematics of oceanic basalts: implications for mantle composition and processes, in *Magmatism in the Ocean Basins edited by AD Saunders and MJ Norry*: Geological Society, London, Special Publication 42, p. 313–345.
- Swinden, HS 1996, The application of volcanic geochemistry to the metallogeny of volcanic-hosted sulphide deposits in central Newfoundland, in *Trace element geochemistry of volcanic rocks: application for massive sulphide exploration edited by DA Wyman*: Geological Association of Canada, Short Course Notes 12, p. 329–358.
- Tyler, IM and Hocking, RM 2001, Tectonic units of Western Australia: Geological Survey of Western Australia, 1:2 500 000 scale map.
- Watkins, PJ and Nolan, J 1990, Determination of rare earth elements, scandium, yttrium and hafnium in 32 georeference materials using inductively coupled plasma-atomic emission spectrometry: *Geostandards Newsletter*, v. 14, p. 11–20.
- Wilde, SA 1980, The Imperding Metamorphic Belt in the Toodyay area and the Balingup Metamorphic Belt and associated granitic rocks of the southwestern Yilgarn Block, in *2IAS Excursion Guide: Geological Society of Australia (W.A. Division); 2nd International Archaeological Symposium*, Perth, Western Australia, 41p.
- Wilde, SA and Walker, IW 1984, Pemberton – Irwin Inlet, WA Sheet SI50-10 and part of Sheet SI50-14: Geological Survey of Western Australia, 1:250 000 Geological Series.
- Winchester, JA and Floyd, PA 1977, Geochemical discrimination of different magma series and their differentiation products using immobile elements: *Chemical Geology*, v. 20, p. 325–343.
- Wood, DA 1980, The application of a Th–Hf–Ta diagram to problems of tectonomagmatic classification and to establishing the nature of crustal contamination of basaltic lavas of the British Tertiary volcanic province: *Earth and Planetary Science Letters*, v. 50, p. 11–30.
- Wood, DA, Joron, J-L and Treuil, M 1979, A re-appraisal of the use of trace elements to classify and discriminate between magma series erupted in different tectonic settings: *Earth and Planetary Science Letters*, v. 45, p. 326–336.
- Zaleski, E, Froese, E and Gordon, TM 1991, Metamorphic petrology of Fe–Zn–Mg–Al alteration at the Linda volcanogenic massive sulfide deposit, Snow Lake, Manitoba: *Canadian Mineralogist*, v. 29, p. 995–1017.

This Record is published in digital format (PDF) and is available as a free download from the DMIRS website at  
<[www.dmp.wa.gov.au/GSWApublications](http://www.dmp.wa.gov.au/GSWApublications)>.

Further details of geological products produced by the Geological Survey of Western Australia can be obtained by contacting:

Information Centre  
Department of Mines, Industry Regulation and Safety  
100 Plain Street  
EAST PERTH WESTERN AUSTRALIA 6004  
Phone: +61 8 9222 3459 Fax: +61 8 9222 3444  
[www.dmp.wa.gov.au/GSWApublications](http://www.dmp.wa.gov.au/GSWApublications)

METAMORPHOSED VMS MINERALIZATION AT WHEATLEY,  
SOUTHWEST WESTERN AUSTRALIA

